Hindawi
Shock and Vibration
Volume 2023, Article ID 1969500, 19 pages
https://doi.org/10.1155/2023/1969500

Research Article

On a New Three-Dimensional Chaotic System with Adaptive Control and Chaos Synchronization

Nasser A. Saeed[1,2,3] **Hend A. Saleh,**[4] **Wedad A. El-Ganaini,**[1] **Magdi Kamel,**[1] **and Mohamed S. Mohamed**[5]

[1]*Department of Physics and Engineering Mathematics, Faculty of Electronic Engineering, Menouf 32952, Menoufia University, Egypt*
[2]*Mathematics Department, Faculty of Science, Galala University, Galala City 43511, Egypt*
[3]*Department of Automation Biomechanics and Mechatronics, Faculty of Mechanical Engineering, Lodz University of Technology, 90924 Lodz, Poland*
[4]*Department of Basic Science, Menoufia Higher Institute of Engineering and Technology, El-Bagour 32821, Egypt*
[5]*Department of Mathematics and Statistics, College of Science, Taif University, P.O. Box 11099, Taif 21944, Saudi Arabia*

Correspondence should be addressed to Nasser A. Saeed; nasser.a.saeed@el-eng.menofia.edu.eg

Received 29 December 2022; Revised 19 March 2023; Accepted 1 April 2023; Published 14 April 2023

Academic Editor: Antonio Batista

A three-dimensional autonomous deterministic chaotic system having six parameters is explored within this article. The dynamical characteristics of the proposed system are investigated through eigenvalues structure, bifurcation diagrams, Kaplan–Yorke dimension, Lyapunov exponents, time response, and phase plane trajectories. For the suitable design of the system parameters, it is found that the system can exhibit periodic, period-n, or chaotic oscillations. Accordingly, the system's dynamical behavior to the variation of its coefficients has been explored. The obtained results revealed that the proposed dynamical system does not lose its chaotic oscillations for the small fluctuations of one or more of the values of its parameters. In addition, chaos control and chaos synchronization have been studied by means of the adaptive control strategy relying on Lyapunov's second method of stability. The numerical simulation revealed that superior chaos control and master-slave synchronization have been achieved by the applied control laws. Finally, the obtained results have been simulated via a nonlinear electronic circuit that demonstrated the feasibility of the purposed chaotic system for different engineering applications such as secure communications, cryptosystems, image encryption, and image processing.

1. Introduction

The chaos theory is defined as a branch of computer science and mathematics that studies the dynamical properties of nonlinear systems which are extremely sensitive to the initial conditions [1, 2]. Lyapunov exponents and the compactness property of the phase space are the most two important and necessary measures that may be used to investigate the chaotic behavior of such systems. Some of the initial paradigms of the three-dimensional chaotic oscillators in the literature are the Lorenz system [3], Rössler oscillator [4], Arneodo et al. system [5], Sprott system [6], Chen and Ueta oscillator [7], Lü and Chen system [8], Liu et al. system [9], Cai and Tan system [10], Chen and Lee system [11], and Tigan and Opris [12]. Recently, chaotic dynamics has found many applications in different areas such as mechanical systems [13, 14], microelectromechanical systems [15], radar systems [16], vehicle models [17], random number generators [18], robotic systems [19–22], memristive devices [23–25], maglev systems [26], rotor active magnetic bearings systems [27–29], biodynamics [30], biological systems [31–34], ecological systems [35, 36], cardiology [37, 38], chemical reactions [39–42], lasers [43, 44], unmanned aerial vehicles [45], rotating machinery [46–50], secure communications [51–53], image encryption [54–56], cryptosystems [57, 58], financial system [59–61], DC motor systems [62], and electronic circuits [63–65]. Any chaotic attractor has an infinite number of unstable periodic orbits. Therefore, chaotic motion arises when the system states move in the neighborhood of one of these unstable periodic orbits for a short period and then fall close to another unstable periodic orbit for a limited time and so forth. This mechanism results in unpredictable motion of the system state for a long time, where this motion is called chaotic oscillation. Chaos control aims to stabilize the chaotic wandering of the system states about its equilibrium points. Many control techniques have been applied for this purpose such as the optimal control system [66, 67], state-feedback control [68], sliding mode and integral sliding mode control [69–74], backstepping control method [75], adaptive control [76–78], and time-delayed feedback control [79].

Chaotic synchronization is a phenomenon that happens when two or more oscillators are coupled or when an oscillator drives another one. The common meaning of synchronization is that the phases of two or more systems change according to a specific pattern. The synchronization phenomenon is abundant in nature, science, social life, and engineering. Well-known systems such as clocks, firing neurons, applauding audiences, singing crickets, and cardiac pacemakers tend to operate in synchrony [80]. There are five synchronization techniques, which are phase synchronization, generalized synchronization, lag synchronization, amplitude envelope synchronization, anticipated synchronization, and complete synchronization. A complete synchronization regime is the common one that is used with a pair of chaotic systems known as the master system and the slave one. The main target of this synchronization technique is to force the slave system output according to a specific control law to track the output of the master system. Pecora and Carroll are the first people that found chaos synchronization in their experiments on circuits [81, 82], where the authors utilized two Lorenz systems where one of them has been used as the master system and the other as the slave. They found that the synchronization among the master and slave systems occurred when the first state variable of the slave system is replaced with the first state variable of the master system. This synchronization scheme is called the P-C scheme. In fact, many control techniques that are used for chaos control can also be utilized in chaos synchronization, where the active control method has been applied in chaos synchronization when all the system parameters are measurable [83–87]. The adaptive control strategy is also employed in chaotic system synchronization when some or all the system parameters are not measurable or when the estimation for some uncertain parameters is required [88–91]. In addition, sampled data feedback control strategies [92–94], time-delayed feedback control techniques [95, 96], and backstepping control methods [97, 98] are used in the chaos synchronization. Moreover, the sliding mode control has been applied extensively in chaos synchronization [99, 100].

In general, 3D-chaotic systems can be categorized depending on the number of terms, parameters, and equilibrium points as shown in Table 1 [101–108]. Also, the chaotic system with dimensions higher than 3D and having at least two positive Lyapunov exponents is called a hyperchaotic system [109, 110].

Within this article, a new 3D-chaotic system with four linear terms, two quadratic nonlinear terms, and six parameters is presented. Detailed bifurcation analysis for the considered system has been conducted through the time response, phase plane trajectories, Lyapunov exponents, bifurcation diagrams, and Kaplan–Yorke dimension. The fluctuation of the different system parameters on the system's dynamics is explored. The obtained results illustrated that the considered system may respond with periodic, period-n, or chaotic oscillations depending on the values of its parameters. Accordingly, the optimal values of the system parameters are designed in such a way that makes the considered system oscillate chaotically, where both the Lyapunov exponents and the corresponding Kaplan–Yorke dimension are obtained. In addition, chaos control has been achieved by designing an adaptive controller based on Lyapunov's second method of stability. Moreover, the chaos synchronization of the introduced chaotic system with itself as a master-slave system has been investigated by designing a globally stable adaptive control system. Finally, we have built an electronic circuit using MultiSim (version 13.0) to simulate the chaotic dynamics of the considered system.

2. The Novel 3D Chaotic System

The study of chaos arose from the discovery of the well-known Lorenz system in 1963. A chaotic system is a nonlinear dynamical system that is very sensitive to the initial conditions and produces aperiodic bounded signals that resemble noise despite not being generated from stochastic systems. The breakthrough of the huge applications of chaos (as in mathematics, computer science, engineering, population dynamics, robotics, biology, and so on) has prompted chaos generation to be a vital research subject. Therefore, this article introduces a novel 3D-chaotic autonomous system with four linear terms and two quadratic terms as follows.

$$\begin{aligned}
\dot{x} &= -ax + by^2, \\
\dot{y} &= ry - gz, \\
\dot{z} &= -fz + cxy,
\end{aligned} \tag{1}$$

where $x, y,$ and z denote the state variables and $a, b, c, f, g,$ and r are positive constant parameters that form the coefficients of the considered system. At the system parameters $a = 2, b = 7, c = 5, f = 8, g = 11,$ and $r = 4$, system (1) exhibits complex dynamics. The chaotic motion of the

Table 1: Categorization of the different 3D-chaotic systems.

3D chaotic systems	No. of terms	No. of parameters	State of equilibria	References
$\dot{\mathbf{x}} = \mathbf{a}(\mathbf{y}-\mathbf{x}) + \mathbf{byz}^2$, $\dot{\mathbf{y}} = \mathbf{cx} + \mathbf{dxz}^2$, $\dot{\mathbf{z}} = \mathbf{hz} + \mathbf{kx}^2$.	7	6	Five equilibrium points	2013 [101]
$\dot{\mathbf{x}} = -\mathbf{x} - 2\mathbf{y}$, $\dot{\mathbf{y}} = -\mathbf{xz} - \mathbf{by} - \mathbf{ax}$, $\dot{\mathbf{z}} = \mathbf{xy} - \mathbf{cz}$.	7	4	Three equilibrium points	2014 [102]
$\dot{\mathbf{x}} = \mathbf{y} + \mathbf{ax} + \mathbf{bxz}$, $\dot{\mathbf{y}} = \mathbf{cxz} + \mathbf{dx} + \mathbf{yz} + \mathbf{1}$, $\dot{\mathbf{z}} = \mathbf{1} + \mathbf{xy}$.	9	4	Three equilibrium points	2016 [103]
$\dot{\mathbf{x}} = \mathbf{y} - \mathbf{x} - \mathbf{az}$, $\dot{\mathbf{y}} = \mathbf{xz} - \mathbf{x}$, $\dot{\mathbf{z}} = -\mathbf{xy} - \mathbf{y} + \mathbf{b}$.	8	2	Three equilibrium points	2012 [104]
$\dot{\mathbf{x}} = \mathbf{wx} - \mathbf{y}^2$, $\dot{\mathbf{y}} = \mu(\mathbf{z}-\mathbf{y})$, $\dot{\mathbf{z}} = \alpha\mathbf{y} - \beta\mathbf{z} + \mathbf{xy}$.	7	4	Three equilibrium points	2016 [105]
$\dot{\mathbf{x}} = \mathbf{a}(\mathbf{y}-\mathbf{x})$, $\dot{\mathbf{y}} = \mathbf{bx} - \mathbf{cxz}$, $\dot{\mathbf{z}} = \mathbf{e}^{\mathbf{xy}} - \mathbf{dz}$.	6	4	Two equilibrium points	2012 [106]
$\dot{\mathbf{x}} = \mathbf{a}(\mathbf{y}-\mathbf{x})$, $\dot{\mathbf{y}} = (\mathbf{c}-\mathbf{a})\mathbf{x} - \mathbf{xz} + \mathbf{cy}$, $\dot{\mathbf{z}} = \mathbf{xy} - \mathbf{bz}$.	8	3	Three equilibrium points	2002 [8]
$\dot{\mathbf{x}} = \mathbf{a}(\mathbf{y}-\mathbf{x})$, $\dot{\mathbf{y}} = \mathbf{bx} - \mathbf{kxz}$, $\dot{\mathbf{z}} = -\mathbf{cz} + \mathbf{hx}^2$.	6	5	Three equilibrium points	2004 [9]
$\dot{\mathbf{x}} = \mathbf{a}(\mathbf{y}-\mathbf{x})$, $\dot{\mathbf{y}} = \mathbf{bx} + \mathbf{cy} - \mathbf{xz}$, $\dot{\mathbf{z}} = \mathbf{x}^2 - \mathbf{hz}$.	7	4	Three equilibrium points	2007 [10]
$\dot{\mathbf{x}} = -\mathbf{ax} + \mathbf{by}^2$, $\dot{\mathbf{y}} = \mathbf{ry} - \mathbf{gz}$, $\dot{\mathbf{z}} = -\mathbf{fz} + \mathbf{cxy}$.	6	6	Three equilibrium points	This paper

suggested dynamical system will be proved in the flowing subsections.

2.1. Dissipativity, Attractor Existence, and Equilibrium Points. The nonlinear autonomous system given by equation (1) can be expressed in the state-space form as follows:

$$W(x,y,z) = \begin{bmatrix} w_1(x,y,z) \\ w_2(x,y,z) \\ w_3(x,y,z) \end{bmatrix} = \begin{bmatrix} -ax + by^2 \\ ry - gz \\ -fz + cxy \end{bmatrix}. \quad (2)$$

According to equation (2), the divergence of the vector field $W(x,y,z)$ on R^3 can be calculated simply as follows:

$$\operatorname{div}(W) = \frac{\partial w_1}{\partial x} + \frac{\partial w_2}{\partial y} + \frac{\partial w_3}{\partial z} = -a + r - f. \quad (3)$$

Therefore, the necessary and sufficient conditions for the nonlinear autonomous system given by equation (1) to be a dissipative one are that the divergence $\operatorname{div}(W)$ should be a negative value. So, based on equation (3), system (1) is a dissipative system if and only if $-a + r - f < 0$.

Suppose Ω is a region in R^3 with smooth boundaries and let $\Omega(t) = \varphi_t(\Omega)$, where φ_t represents the flow of the vector field W. Let $F(t)$ represent the volume of $\Omega(t)$. According to the Liouville theorem [111], we have

$$\begin{aligned} \frac{dF(t)}{dt} &= \int_{\Omega(t)}^{-} \operatorname{div}(W) \mathrm{d}x\, \mathrm{d}y\, \mathrm{d}z \\ &= (-a + r + f)\int_{\Omega(t)} \mathrm{d}x\, \mathrm{d}y\, \mathrm{d}z = (-a + r - f)F(t). \end{aligned} \quad (4)$$

The solution of equation (4) can be written as $F(t) = F_0 e^{(-a+r-f)t}$. Therefore, any volume element F_0 in the space of system (1) will be contracted by the flow into the volume element $F_0 e^{(-a+r-f)t}$ at the time t. This means that each volume containing the system trajectories will be shrunk to zero when $t \longrightarrow \infty$ at an exponential decay rate $-a + r - f$. Accordingly, all the orbits of the system given by equation (1) will be confined into a subset of zero volume, and the asymptotic motion of the system will settle into an attractor regardless of the initial conditions. So, for the designed parameters ($a = 2, f = 8,$ and $r = 4$), the exponential contraction rate of the considered system is $-6t$. In addition, the equilibrium points of the considered system are $E_1(0,0,0)$, $E_2(\mathrm{fr}/\mathrm{cg}, \sqrt{\mathrm{afr}/\mathrm{cbg}}, r/g\sqrt{\mathrm{afr}/\mathrm{cbg}})$, and $E_3(fr/cg, -\sqrt{\mathrm{afr}/\mathrm{cbg}}, -r/g\sqrt{\mathrm{afr}/\mathrm{cbg}})$. These equilibrium points are unstable when the system parameters are designed such that $a = 2, b = 7, c = 5, r = 4, g = 11,$ and $f = 8$. Thus, the trajectories of the considered dynamical system (1) will diverge from the equilibrium points as long as the initial conditions do not satisfy one of these points.

2.2. Kaplan–Yorke Dimension. Within this section, Lyapunov exponents (LE) of the considered dynamical system are obtained numerically as shown in Figure 1 at the system parameters: $a = 2, b = 7, c = 5, r = 4, g = 11$, and $f = 8$. It is clear from the figure that the steady-state Lyapunov exponents of the considered system are $\mathrm{LE}_1 = 0.5, \mathrm{LE}_2 = 0$, and $\mathrm{LE}_3 = -6.5$, where $\mathrm{LE}_1 < \mathrm{LE}_2 < \mathrm{LE}_3$. Accordingly, one can find the Kaplan–Yorke dimension (i.e., D_{KY}) as follows:

$$D_{\mathrm{KY}} = 2 + \frac{LE_1 + LE_2}{|LE_3|} = 2 + \frac{0.5 + 0.0}{6.5} = 2.0769. \quad (5)$$

It is clear from equation (5) that the considered system has a fractional dimension, which confirms that the considered autonomous dissipative system has a nonperiodic solution.

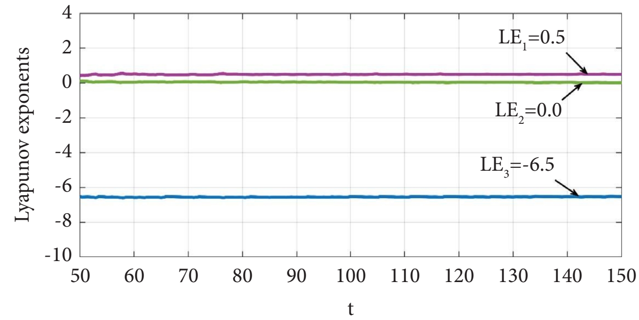

Figure 1: Evolution of the system Lyapunov exponents (i.e., LE) on the time interval $50 \leq 0 < 150$ at $a = 2, b = 7, c = 5, f = 8, g = 11$, and $r = 4$, where the steady-state Lyapunov exponents are $\mathrm{LE}_1 = 0.5, \mathrm{LE}_2 = 0.0$, and $\mathrm{LE}_3 = -6.5$.

2.3. Chaotic Response and Phase Trajectories. Based on the obtained Lyapunov exponents ($LE_1 = 0.5, LE_2 = 0.0$, and $LE_3 = -6.5$) as shown in Figure 1, the autonomous dynamical system (1) will respond with a chaotic bounded motion for any initial conditions in the three-dimensional space except the three equilibrium points $E_1 = (0, 0, 0), E_2 = (0.5818, 0.4077, 0.1483)$, and $E_3 = (0.5818, -0.4077, -0.1483)$. The time response of the considered chaotic system is illustrated in Figure 2 at the initial conditions $x(0) = y(0) = z(0) = 0.01$, while Figure 3 shows the corresponding phase plane trajectories. Figures 2 and 3 are obtained via solving equation (1) numerically using the ODE45 MATLAB solver when $a = 2, b = 7, c = 5, r = 4, g = 11$, and $f = 8$. It is clear from Figure 2 that the system motion is chaotic. In addition, Figure 3 shows that the suggested chaotic system has chaotic attractors with shapes that are different from those Lorenz-like systems.

3. Bifurcation Analysis

For the practical realization of the considered chaotic system, it should have high immunity to the slight fluctuations of one or more of its parameters. Therefore, this section aims to investigate the system dynamics when changing each one of the system parameters. Figure 4 shows the bifurcation diagram and the corresponding Lyapunov exponents utilizing a as a bifurcation parameter along the range $0 < a < 3$, with fixing the other parameters constant. Figure 4(a) illustrates that the system has dissipativity behaviors, where the contractions exponent $-a + r - f < 0$ on the interval $0 < a < 3$. However, Figures 4(a) and 4(b) demonstrate that system motion may be either periodic, period-n, or chaotic depending on the value of the parameter a. Also, one can notice from Figure 4(b) that the system can perform chaotic oscillation at a wide range of about $a = 2$ (i.e., the system oscillates chaotically as long as $1.5 < a < 3$), which guarantees the immunity of the proposed chaotic system to the fluctuation of a without losing its chaotic dynamics.

Figure 5 illustrates the bifurcation of the system motion and the corresponding Lyapunov exponents when utilizing r as a bifurcation parameter on the interval $2 < r < 6$. Figure 5(a) demonstrates that the system may perform periodic oscillations as long as $2 < r < 2.5$, but increasing r beyond 2.5 may result in a periodic-doubling bifurcation, that is, the route to a chaotic motion. In addition, the figure shows that the system may lose its chaotic oscillation via periodic-halving bifurcation if r is increased beyond 5. However, Figure 5(b) confirms that the proposed system can exhibit chaotic motion as long as $3.5 < r < 4.5$, which guarantees the system immunity for the small fluctuation of r about the designed value $r = 4$.

Figure 6 depicts the motion bifurcation and the corresponding Lyapunov exponents when utilizing f as the main bifurcation parameters along the interval $5 < f < 9$. Figure 6(a) shows that the system can perform periodic motion as long as $5 < f < 6$. But, increasing f beyond 6 results in periodic-doubling bifurcation, which ultimately leads to chaotic oscillations as shown in Figure 6(b) when $7 < f \leq 9$. Accordingly, one can confirm the system's immunity to the small fluctuation of f about the designed value $f = 8$. Figures 7–9 are a repetition of Figures 4–6 but concerning the rest of the system parameters b, c, and g, respectively. By examining Figures 4–6, one can demonstrate that the motion bifurcation and the corresponding Lyapunov exponent of the considered chaotic system are insensitive to the variation of the parameters b, c, and g on the intervals $5 < b < 8, 3 < c < 6$, and $9 < g < 12$. Based on the abovementioned investigations, it is clear that the introduced system (1) with the designed parameter values (i.e., $a = 2, b = 7, c = 5, r = 4, g = 11$, and $f = 8$) has high immunity for the slight fluctuations of the values of its parameters.

4. Chaos Control

4.1. Adaptive Controller Design. Chaos control of the proposed dynamical system has been investigated within this section utilizing an adaptive control strategy. Thus, the suggested controlled chaotic system (1) is modified to become

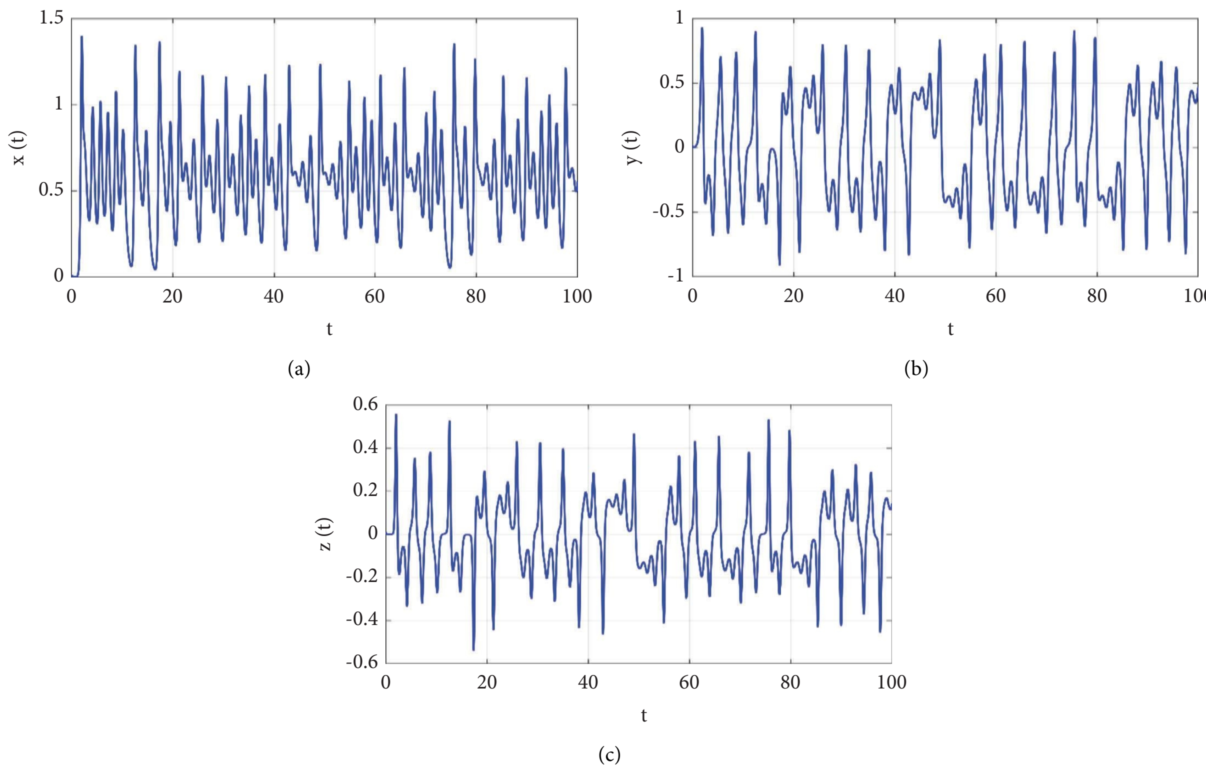

Figure 2: (a–c) Time response of the proposed chaotic system at $x(0) = y(0) = z(0) = 0.01$, $a = 2, b = 7, c = 5, f = 8, g = 11$, and $r = 4$.

$$\begin{aligned}\dot{x} &= -ax + by^2 + u_1,\\ \dot{y} &= ry - gz + u_2,\\ \dot{z} &= -fz + cxy + u_3,\end{aligned} \quad (6)$$

where u_1, u_2, and u_3 are the suggested adaptive control signals to stabilize the chaotic motion of system (1). The main strategy of the adaptive controller is to generate control signals u_1, u_2, and u_3 in order to cancel the nonlinearity of the considered chaotic system (6) and force it to respond as a dissipative linear system with $(0, 0, 0)$ stable equilibrium point. Accordingly, u_1, u_2, and u_3 are designed such that

$$\begin{aligned}u_1 &= \tilde{a}x - \tilde{b}y^2 - \delta_1 x,\\ u_2 &= -\tilde{r}y + \tilde{g}z - \delta_2 y,\\ u_3 &= \tilde{f}z - \tilde{c}xy - \delta_3 z,\end{aligned} \quad (7)$$

where δ_1, δ_2, and δ_3 are positive constants that form the linear feedback gains, while $\tilde{a}, \tilde{b}, \tilde{r}, \tilde{g}, \tilde{f}$, and $\tilde{c}$ denote the estimated parameters of the system coefficients a, b, r, g, f, and c. Now, by substituting equation (7) into equation (6), we have the following controlled system:

$$\begin{aligned}\dot{x} &= -(a - \tilde{a})x + (b - \tilde{b})y^2 - \delta_1 x,\\ \dot{y} &= (r - \tilde{r})y - (g - \tilde{g})z - \delta_2 y,\\ \dot{z} &= -(f - \tilde{f})z + (c - \tilde{c})xy - \delta_3 z.\end{aligned} \quad (8)$$

Notice that when the estimated parameters (i.e., $\tilde{a}, \tilde{b}, \tilde{r}, \tilde{g}, \tilde{f}$, and $\tilde{c}$) reach the same values of the system parameters (i.e., a, b, r, g, f, and c), equation (8) becomes $\dot{x} = -\delta_1 x$, $\dot{y} = -\delta_2 y$, and $\dot{z} = -\delta_3 z$. Accordingly, let us denote the error estimation of the parameters as follows:

$$\begin{aligned}e_1 &= a - \tilde{a}, e_2 = b - \tilde{b}, e_3 = r - \tilde{r}, e_4\\ &= g - \tilde{g}, e_5 = f - \tilde{f}, e_6 = c - \tilde{c}.\end{aligned} \quad (9)$$

Based on equation (9), the derivatives of the parameter estimation errors can be expressed as follows:

$$\dot{e}_1 = -\dot{\tilde{a}}, \dot{e}_2 = -\dot{\tilde{b}}, \dot{e}_3 = -\dot{\tilde{r}}, \dot{e}_4 = -\dot{\tilde{g}}, \dot{e}_5 = -\dot{\tilde{f}}, \dot{e}_6 = -\dot{\tilde{c}}. \quad (10)$$

Substituting equation (9) into equation (8) yields

$$\begin{aligned}\dot{x} &= -e_1 x + e_2 y^2 - \delta_1 x,\\ \dot{y} &= e_3 y - e_4 z - \delta_2 y,\\ \dot{z} &= -e_5 z + e_6 xy - \delta_3 z.\end{aligned} \quad (11)$$

To obtain the control law that will adjust the parameter estimations, let us build up the Lyapunov positive definite function $V_1(x, y, z, e_1, e_2, e_3, e_4, e_5, e_6)$ for the controlled chaotic system given by equation (11) as follows:

$$\begin{aligned}&V_1(x, y, z, e_1, e_2, e_3, e_4, e_5, e_6)\\ &\quad = \frac{1}{2}\left(x^2 + y^2 + z^2 + e_1^2 + e_2^2 + e_3^2 + e_4^2 + e_5^2 + e_6^2\right).\end{aligned} \quad (12)$$

Differentiating the constructed Lyapunov function $V_1(x, y, z, e_1, e_2, e_3, e_4, e_5, e_6)$, we have

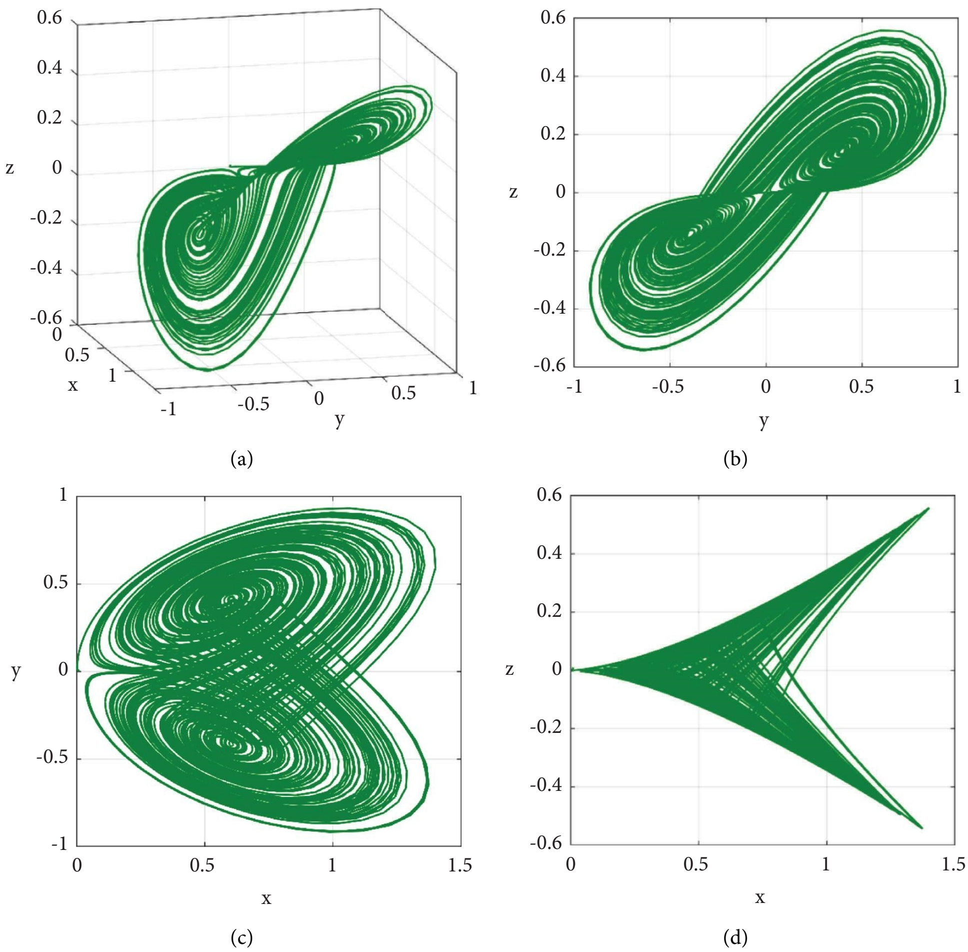

FIGURE 3: Phase plane trajectories of the system when $a = 2, b = 7, c = 5, f = 8, g = 11,\ r = 4$ and $x(0) = y(0) = z(0) = 0.01$: (a) Three-dimensional phase trajectory in (x, y, z) and (b–d) two-dimensional phase trajectory in (y, z), (x, y), and (x, z), respectively.

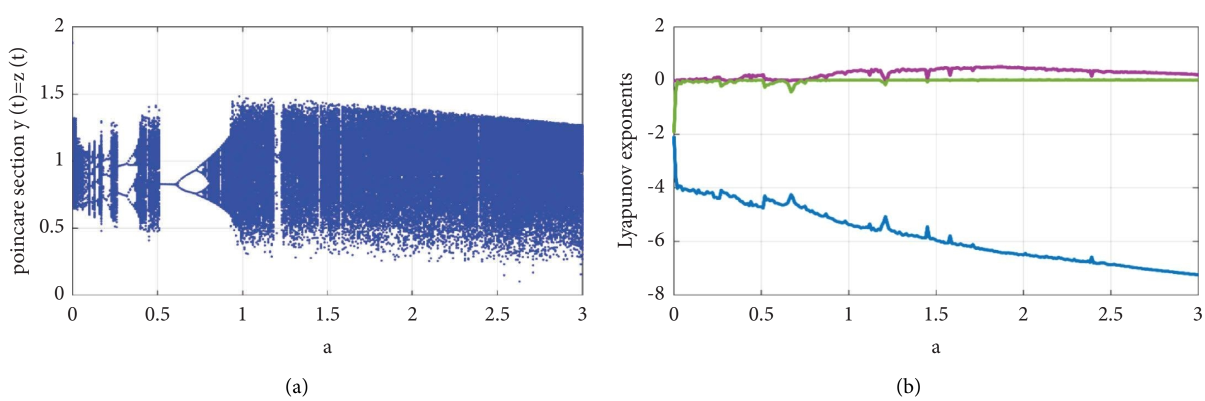

FIGURE 4: (a) The system bifurcation diagram and (b) the corresponding Lyapunov exponents, utilizing a as the bifurcation parameter with fixing the other parameters constant such that $b = 7, c = 5, f = 8, g = 11,$ and $r = 4$.

$$\dot{V}_1(x, y, z, e_1, e_2, e_3, e_4, e_5, e_6) = (x\dot{x} + y\dot{y} + z\dot{z} + e_1\dot{e}_1 + e_2\dot{e}_2 + e_3\dot{e}_3 + e_4\dot{e}_4 + e_5\dot{e}_5 + e_6\dot{e}_6). \tag{13}$$

Eliminating $\dot{x}, \dot{y}, \dot{z}, \dot{e}_1, \dot{e}_2, \dot{e}_3, \dot{e}_4, \dot{e}_5$ and $\dot{e}_6$ from equation (13) utilizing equations (10) and (11) yields

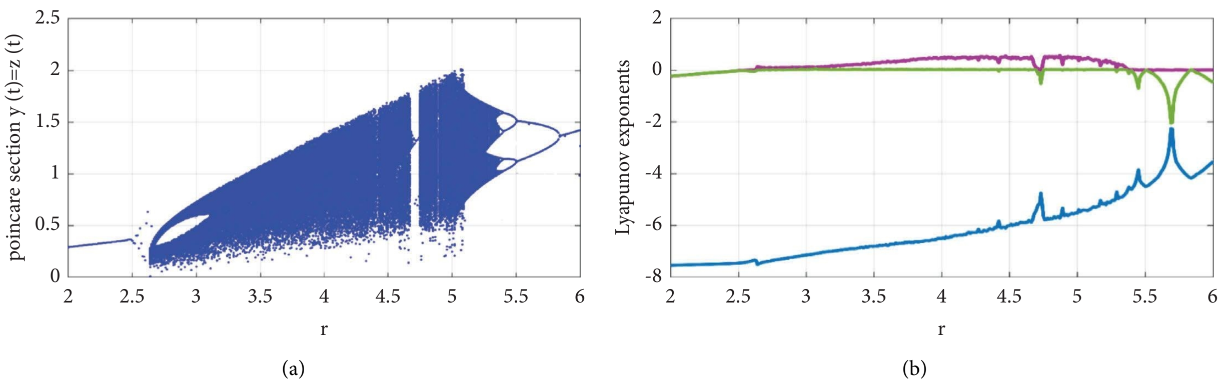

FIGURE 5: (a) The system bifurcation diagram and (b) the corresponding Lyapunov exponents, utilizing r as a bifurcation parameter with fixing the other parameters constant such that $a = 2, b = 7, c = 5, f = 8,$ and $g = 11$.

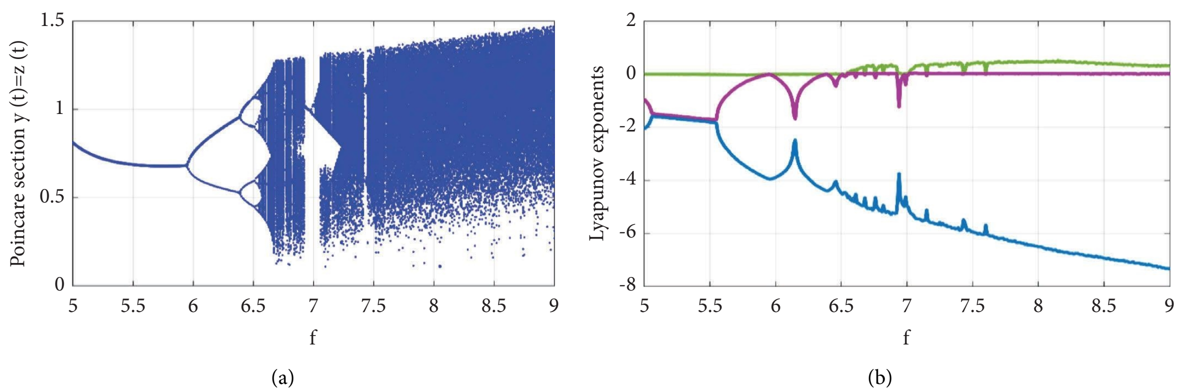

FIGURE 6: (a) The system bifurcation diagram and (b) the corresponding Lyapunov exponents, utilizing f as a bifurcation parameter with fixing the other parameters constant such that $a = 2, b = 7, c = 5, g = 11,$ and $r = 4$.

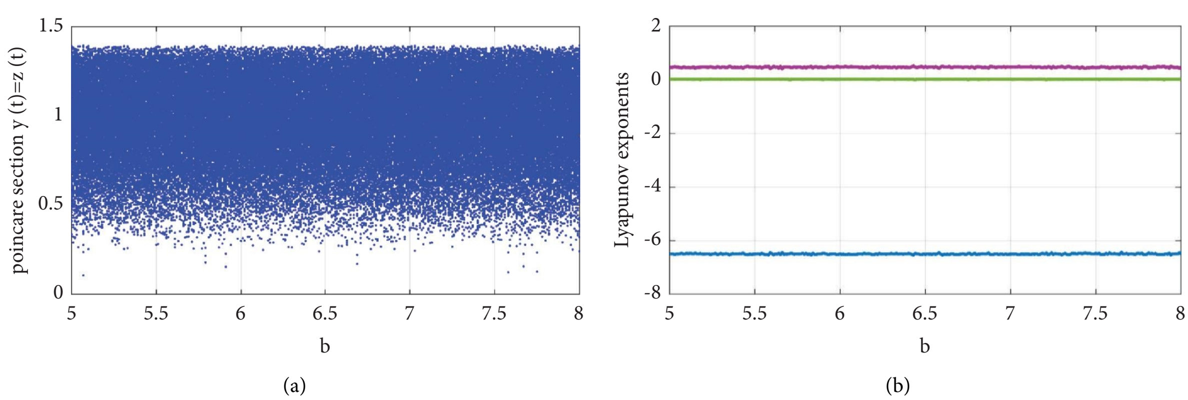

FIGURE 7: (a) The system bifurcation diagram and (b) the corresponding Lyapunov exponents, utilizing b as the bifurcation parameter with fixing the other parameters constant such that $a = 2, c = 5, f = 8, g = 11,$ and $r = 4$.

$$\begin{aligned}&\dot{V}_1(x, y, z, e_1, e_2, e_3, e_4, e_5, e_6)\\&=\left(-\delta_1 x^2 - \delta_2 y^2 - \delta_3 z^2 - e_1\left(\dot{\tilde{a}} + x^2\right) - e_2\left(\dot{\tilde{b}} - xy^2\right) - e_3\left(\dot{\tilde{r}} - y^2\right) - e_4\left(\dot{\tilde{g}} + yz\right) - e_5\left(\dot{\tilde{f}} + z^2\right) - e_6\left(\dot{\tilde{c}} - \mathrm{xyz}\right)\right).\end{aligned} \tag{14}$$

According to equation (14), the parameters estimation law can be chosen as follows:

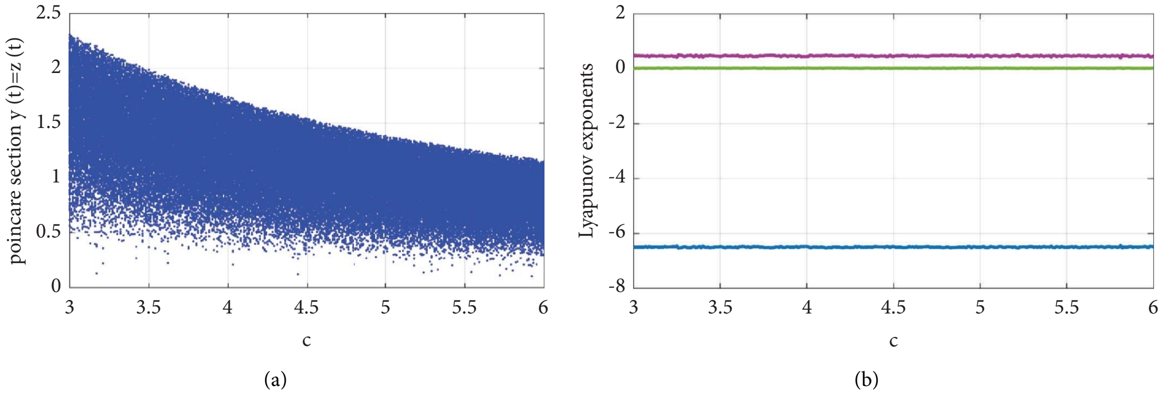

Figure 8: (a) The system bifurcation diagram and (b) the corresponding Lyapunov exponents, utilizing c as the bifurcation parameter with fixing the other parameters constant such that $a = 2, b = 7, f = 8, g = 11$, and $r = 4$.

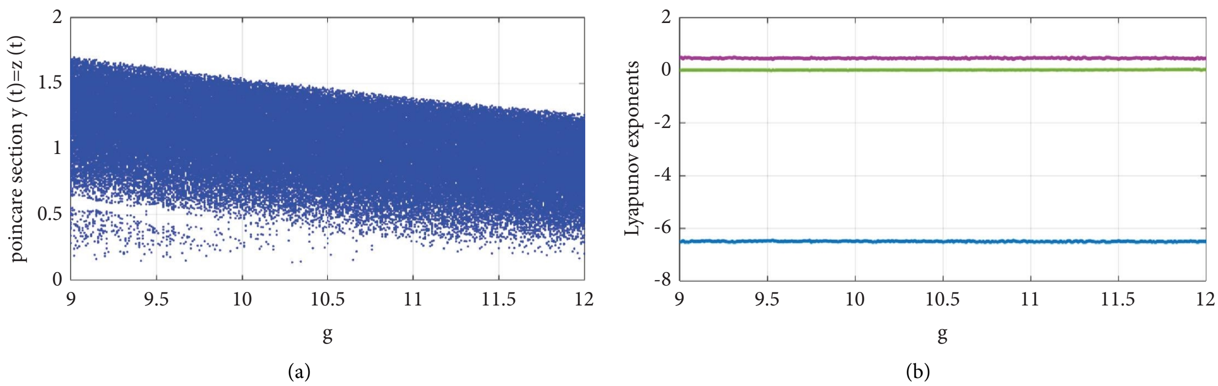

Figure 9: (a) The system bifurcation diagram and (b) the corresponding Lyapunov exponents, utilizing g as the bifurcation parameter with fixing the other parameters constant such that $a = 2, b = 7, c = 5, f = 8$, and $r = 4$.

$$\begin{aligned}
\dot{\tilde{a}} &= -x^2 + \eta_1 (a - \tilde{a}),\\
\dot{\tilde{b}} &= xy^2 + \eta_2 (b - \tilde{b}),\\
\dot{\tilde{r}} &= y^2 + \eta_3 (r - \tilde{r}),\\
\dot{\tilde{g}} &= -yz + \eta_4 (g - \tilde{g}),\\
\dot{\tilde{f}} &= -z^2 + \eta_5 (f - \tilde{f}),\\
\dot{\tilde{c}} &= \mathrm{xyz} + \eta_6 (c - \tilde{c}),
\end{aligned} \tag{15}$$

where η_k $(k = 1, 2, \ldots, 6)$ are positive constants. Based on the designed estimation law given by equation (15), the derivative of the Lyapunov function $\dot{V}_1 (x, y, z, e_1, e_2, e_3, e_4, e_5, e_6)$ is a negative definite function that can be written as follows:

$$\dot{V}_1 (x, y, z, e_1, e_2, e_3, e_4, e_5, e_6) = -\left(\delta_1 x^2 + \delta_2 y^2 + \delta_3 z^2 + \eta_1 e_1^2 + \eta_2 e_2^2 + \eta_3 e_3^2 + \eta_4 e_4^2 + \eta_5 e_5^2 + \eta_6 e_6^2\right). \tag{16}$$

Theorem 1. *The controlled system that is given by equation (6) with the unknown coefficients a, b, r, g, f, and c is globally stabilized regardless of the initial conditions by both the designed control law given by equation (7) and the parameters estimation law given by equation (15), where δ_j $(j = 1, 2, 3)$ and η_k $(k = 1, 2, \ldots, 6)$ are positive constants.*

Proof. The above theorem is a simple consequence of Lyapunov's second method for stability [112]. We showed that the Lyapunov function $V_1 (x, y, z, e_1, e_2, e_3, e_4, e_5, e_6)$ that is given by equations (12) is a positive definite function on R^9. In addition, we illustrated that the first derivative $\dot{V}_1 (x, y, z, e_1, e_2, e_3, e_4, e_5, e_6)$ given by equations (15) is

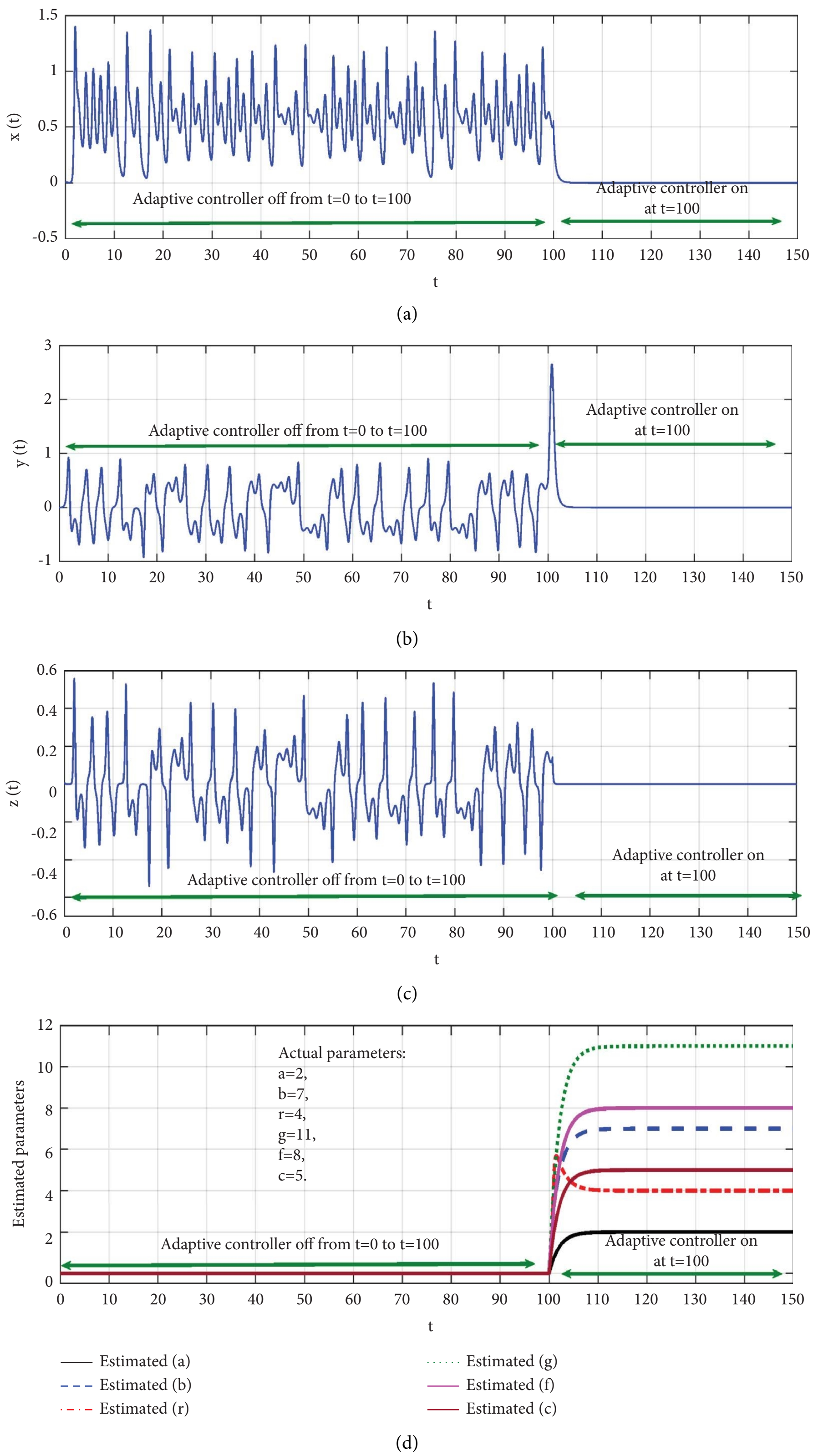

Figure 10: The evolution of the chaotic system time response before and after chaos control when the system parameters $a = 2, b = 7, r = 4, g = 11, f = 8, c = 5,$ control gains $\delta_i = \eta_j = 0.5$, $(i = 1, 2, 3, j = 1, 2, .., 6)$, and initial conditions $x(0) = y(0) = z(0) = 0.01, \tilde{a}(0) = \tilde{b}(0) = \tilde{r}(0) = \tilde{g}(0) = \tilde{f}(0) = \tilde{c}(0) = 0.0$. (a–c) the evolution of the system states $x(t)$, $y(t)$, and $z(t)$ before chaos control on the interval $0 \leq t < 100$ and after control on the interval $100 \leq t \leq 150$, and (d) the evolution of the system estimated parameters $\tilde{a}, \tilde{b}, \tilde{c}, \tilde{g}, \tilde{f}$, and $\tilde{r}$.

a negative definite on R^9. Hence, according to Lyapunov's second method for stability, it follows that the system states $x(t), y(t), z(t), e_1(t), e_2(t), e_3(t), e_4(t), e_5(t)$, and $e_6(t)$ tend to zero exponentially as the time t tends to infinity, which completes the proof that the system given by equation (6) is globally stable. □

4.2. Numerical Simulation of Chaos Adaptive Control. Numerical simulations for the introduced adaptive control system given in Section 4.1 are illustrated within this section. The time response of the controlled chaotic system is simulated numerically via solving equations (6), (7), and (15) using the ODE45 MATLAB solver as in Figure 10 when $a = 2, b = 7, c = 5, f = 8, g = 11, r = 4$, and $\delta_i = \eta_j = 0.5$, $(i = 1, 2, 3, j = 1, 2, \ldots, 6)$ at the initial conditions $x(0) = y(0) = z(0) = 0.01, \tilde{a}(0) = \tilde{b}(0) = \tilde{g}(0) = \tilde{c}(0) = \tilde{f}(0) = \tilde{r}(0) = 0.0$. Figures 10(a)–10(c) show the system's chaotic motion before control on the time interval $0 < t < 100$ and after turning on the introduced adaptive control law at $t = 100$ up to $t = 150$. In addition, Figure 10(d) shows the evolution of the estimated parameters $(\tilde{a}(t), \tilde{b}(t), \tilde{c}(t), \tilde{g}(t), \tilde{f}(t), \tilde{r}(t))$ after turning on the controller at $t = 100$. It is clear from Figures 10(a)–10(c) that the chaotic states $x(t), y(t)$, and $z(t)$ on the interval $0 < t < 100$ have been forced to enter the equilibrium point $E_1(0, 0, 0)$ as soon as turning on the controller at $t = 100$ (i.e., $x(t) \longrightarrow 0, y(t) \longrightarrow 0$, and $z(t) \longrightarrow 0$ as soon as the controller is activated). Moreover, Figure 10(d) demonstrates the exponential convergence of the estimated parameters to the system parameters (i.e., $\tilde{a}(t) \longrightarrow a = 2, \tilde{b}(t) \longrightarrow b = 7, \tilde{c}(t) \longrightarrow c = 5, \tilde{g}(t) \longrightarrow g = 11, \tilde{f}(t) \longrightarrow f = 8, \tilde{r}(t) \longrightarrow r = 4$).

5. Chaos Synchronization

5.1. Adaptive Controller Design. Based on the investigation given in Section 3, the parameters b, c, and g have negligible influence on the system's dynamical behaviors. Accordingly, these parameters are treated as fixed values such that $b = 7, c = 5$, and $g = 11$ within this section. Therefore, the modified novel chaotic system (i.e., equation (1)) that represents the master system is given as follows:

$$\begin{aligned} \dot{x} &= -ax + 7y^2, \\ \dot{y} &= ry - 11z, \\ \dot{z} &= -fz + 5yx. \end{aligned} \tag{17}$$

In addition, let the slave system be given by the following dynamical equation:

$$\begin{aligned} \dot{X} &= -aX + 7Y^2 + U_1, \\ \dot{Y} &= rY - 11Z + U_2, \\ \dot{Z} &= -fZ + 5XY + U_3, \end{aligned} \tag{18}$$

where X, Y, and Z denote the slave system states, and U_1, U_2, and U_3 are the control signals to be designed in order to achieve the global synchronization between the master system (17) and the slave one (18). Accordingly, the master-slave state errors can be defined as follows:

$$e_X = X - x, e_Y = Y - y, e_Z = Z - z. \tag{19}$$

Based on equations (17)–(19), the error dynamics can be defined as follows:

$$\begin{aligned} \dot{e_X} &= -ae_X + 7e_Y^2 + U_1, \\ \dot{e_Y} &= re_Y - 11e_Z + U_2, \\ \dot{e_Z} &= -fe_Z + 5(\mathrm{XY} - \mathrm{xy}) + U_3. \end{aligned} \tag{20}$$

According to equation (20), let us design the control law as follows:

$$\begin{aligned} U_1 &= \hat{a}e_X - 7e_Y^2 - \alpha_1 e_X, \\ U_2 &= -\hat{r}e_Y + 11e_Z - \alpha_2 e_Y, \\ U_3 &= \hat{f}e_Z - 5(\mathrm{XY} - \mathrm{xy}) - \alpha_3 e_Z, \end{aligned} \tag{21}$$

where $\hat{a}, \hat{r}$, and $\hat{f}$ are the estimated parameters of the unknown system parameters a, r, and f. In addition, α_1, α_2, and α_3 are positive constants that represent the control gains. Now, substituting equation (21) into equation (20) yields

$$\begin{aligned} \dot{e_X} &= -e_a e_X - \alpha_1 e_X, \\ \dot{e_Y} &= e_r e_Y - \alpha_2 e_Y, \\ \dot{e_Z} &= -e_f e_Z - \alpha_3 e_Z, \end{aligned} \tag{22}$$

where $e_a = a - \hat{a}, e_r = r - \hat{r}$, and $e_f = f - \hat{f}$ are the parameter estimation errors, and $\dot{e_a} = -\dot{\hat{a}}, \dot{e_r} = -\dot{\hat{r}}, \dot{e_f} = -\dot{\hat{f}}$. To obtain the control laws that will adjust the states' synchronization and the parameter estimations, let us build up the Lyapunov positive definite function $V_2(e_X, e_Y, e_Z, e_a, e_r, e_f)$ for the chaotic system given by equation (22) as follows:

$$V_2(e_X, e_Y, e_Z, e_a, e_r, e_f) = \frac{1}{2}\left(e_X^2 + e_Y^2 + e_Z^2 + e_a^2 + e_r^2 + e_f^2\right). \tag{23}$$

Accordingly, the derivative of equation (23) can be expressed as follows:

$$\begin{aligned} &V_2(e_X, e_Y, e_Z, e_a, e_r, e_f) \\ &\quad = \left(e_X\dot{e_X} + e_Y\dot{e_Y} + e_Z\dot{e_Z} + e_a\dot{e_a} + e_r\dot{e_r} + e_f\dot{e_f}\right). \end{aligned} \tag{24}$$

Eliminating $\dot{e_X}, \dot{e_Y}, \dot{e_Z}, \dot{e_a}, \dot{e_r}$, and $\dot{e_f}$ from equation (24) utilizing equation (22) yields

$$\begin{aligned} &\dot{V}_2(e_X, e_Y, e_Z, e_a, e_r, e_f) \\ &\quad = -\alpha_1 e_X^2 - \alpha_2 e_Y^2 - \alpha_3 e_Z^2 \\ &\qquad - e_a\left(\dot{\hat{a}} + e_X^2\right) - e_r\left(\dot{\hat{r}} - e_Y^2\right) - e_f\left(\dot{\hat{f}} + e_Z^2\right). \end{aligned} \tag{25}$$

According to equation (25), the parameters estimation law can be designed as follows:

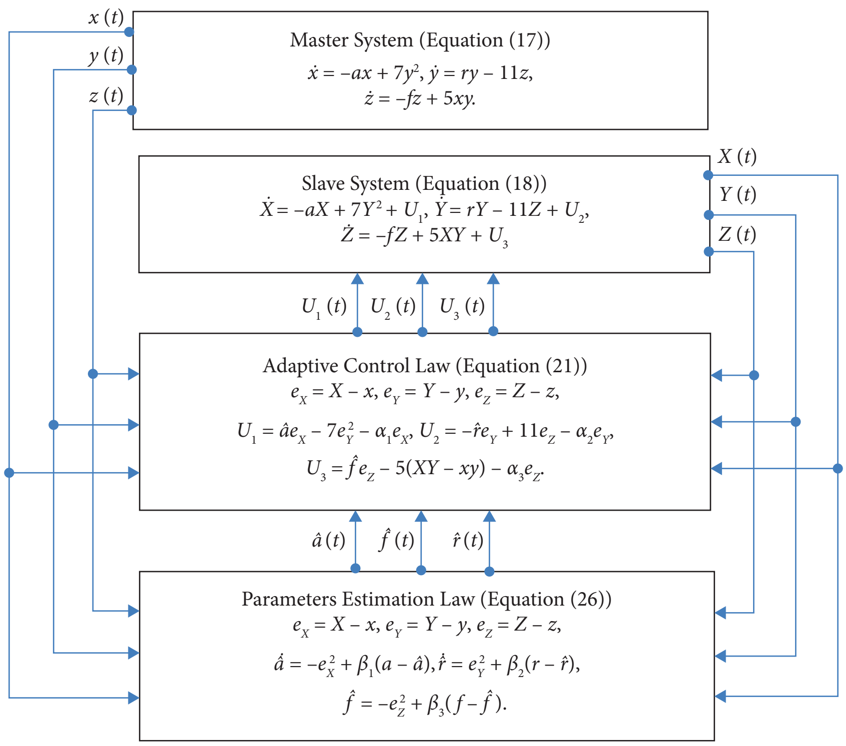

FIGURE 11: Block diagram of the master-slave synchronized chaotic system.

$$\begin{aligned}\dot{\hat{a}} &= -e_X^2 + \beta_1 (a - \hat{a}),\\ \dot{\hat{r}} &= e_Y^2 + \beta_2 (r - \hat{r}),\\ \dot{\hat{f}} &= -e_Z^2 + \beta_3 (f - \hat{f}),\end{aligned} \tag{26}$$

where β_j $(j = 1, 2, 3)$ are positive constants. Based on the designed estimation law given by equation (26), the derivative of the Lyapunov function $\dot{V}_2 (e_X, e_Y, e_Z, e_a, e_r, e_f)$ is a negative definite function that can be expressed as follows:

$$\begin{aligned}&\dot{V}_2\left(e_X, e_Y, e_Z, e_a, e_r, e_f\right)\\ &\quad = -\left(\alpha_1 e_X^2 + \alpha_2 e_Y^2 + \alpha_3 e_Z^2 + \beta_1 e_a^2 + \beta_2 e_r^2 + \beta_3 e_f^2\right).\end{aligned} \tag{27}$$

Theorem 2. *The coupled synchronized master-slave chaotic system that is given by equations (17) and (18) with the unknown coefficients $a, r,$ and f is globally stabilized via both the designed control law given by equation (21) and the updated parameters law that is given by equation (26), where α_j and β_j $(j = 1, 2, 3)$ are positive constants.*

Proof. The abovementioned theorem is a simple consequence of Lyapunov's second method for stability [112]. We designed the Lyapunov function $V_2 (e_X, e_Y, e_Z, e_a, e_r, e_f)$ given by equation (23) to be a positive definite function on R^6. In addition, its first-order derivative (i.e., $\dot{V}_2 (e_X, e_Y, e_Z, e_a, e_r, e_f)$) given by equation (27) is a negative definite on R^6. Therefore, based on Lyapunov's second method for stability, it follows that $e_X (t), e_Y (t), e_Z (t), e_a (t), e_r (t),$ and $e_f (t)$ tend to zero exponentially as the time t tends to infinity, which completes the proof that the master-slave system given by equations (17) and (18) is globally stable. □

5.2. Numerical Simulation of Chaos Synchronization. Based on equations (17)–(19), (21), and (26), the block diagram describing the sequential execution of the synchronized master-slave system is depicted in Figure 11. The figure shows that the chaotic states of both the master and slave systems (i.e., $x (t), y (t), z (t), X (t), Y (t),$ and $Z (t)$) are firstly fed into both the adaptive control law (i.e., equation (21)) and parameters estimation law (i.e., equation (26)) using an appropriate sensors network simultaneously. Then, the parameter estimation law estimates the system parameters $\hat{a} (t), \hat{f} (t),$ and $\hat{r} (t)$ according to the predefined estimation rule (i.e., equation (26)) to feed them into the adaptive control law. After that, the adaptive control law computes the control signals $U_1 (t), U_2 (t),$ and $U_3 (t)$ based on the input signals $x (t), y (t), z (t), X (t), Y (t), Z (t), \hat{a} (t), \hat{f} (t),$ and $\hat{r} (t)$ to apply them to the slave system in order to follow typically the same chaotic motion of the master one.

Accordingly, the master-slave synchronized motion has been simulated within this section via solving equations (17)–(19), (21), and (26) numerically using MATLAB ODE45 solver as shown in Figures 12 and 13 when the system parameters $a = 2, r = 4, f = 8,$ control gains $\alpha_i = \beta_i = 2.0,$ $(i = 1, 2, 3),$ and initial conditions $x (0) = y (0) = z (0) = 0.1, X (0) = Y (0) = Z (0) = 0.0001,$ $\hat{a} (0) = \hat{r} (0) = \hat{f} (0) = 0.0.$ Figures 12(a)–12(c) illustrate the instantaneous oscillations of both the master and slave systems before synchronization (i.e.,

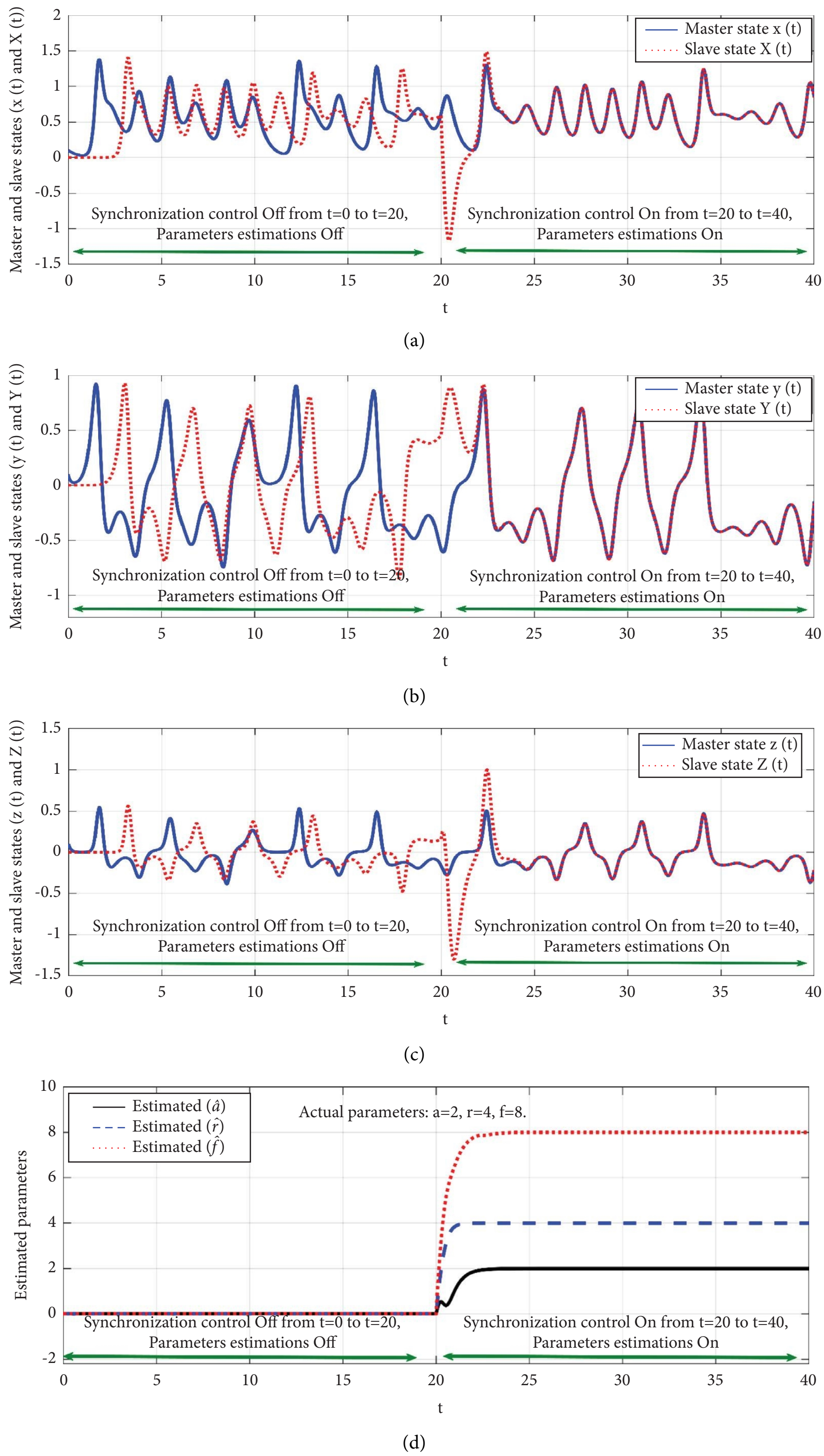

FIGURE 12: The evolution of the system time response before and after chaos synchronization when $a = 2, b = 7, r = 4, g = 11, f = 8, c = 5$, control gains $\alpha_i = \beta_i = 2.0$, $(i = 1, 2, 3)$, and initial conditions $x(0) = y(0) = z(0) = 0.1, X(0) = Y(0) = Z(0) = 0.0001, \hat{a}(0) = \hat{r}(0) = \hat{f}(0) = 0.0$. (a–c) the evolution of both the master-slave systems states $x(t), y(t), z(t), X(t), Y(t)$, and $Z(t)$ before chaos synchronization on $0 \leq t < 20$ and after chaos synchronization on $20 \leq t \leq 40$ and (d) the evolution of the system estimated parameters $\hat{a}, \hat{r}$, and $\hat{f}$.

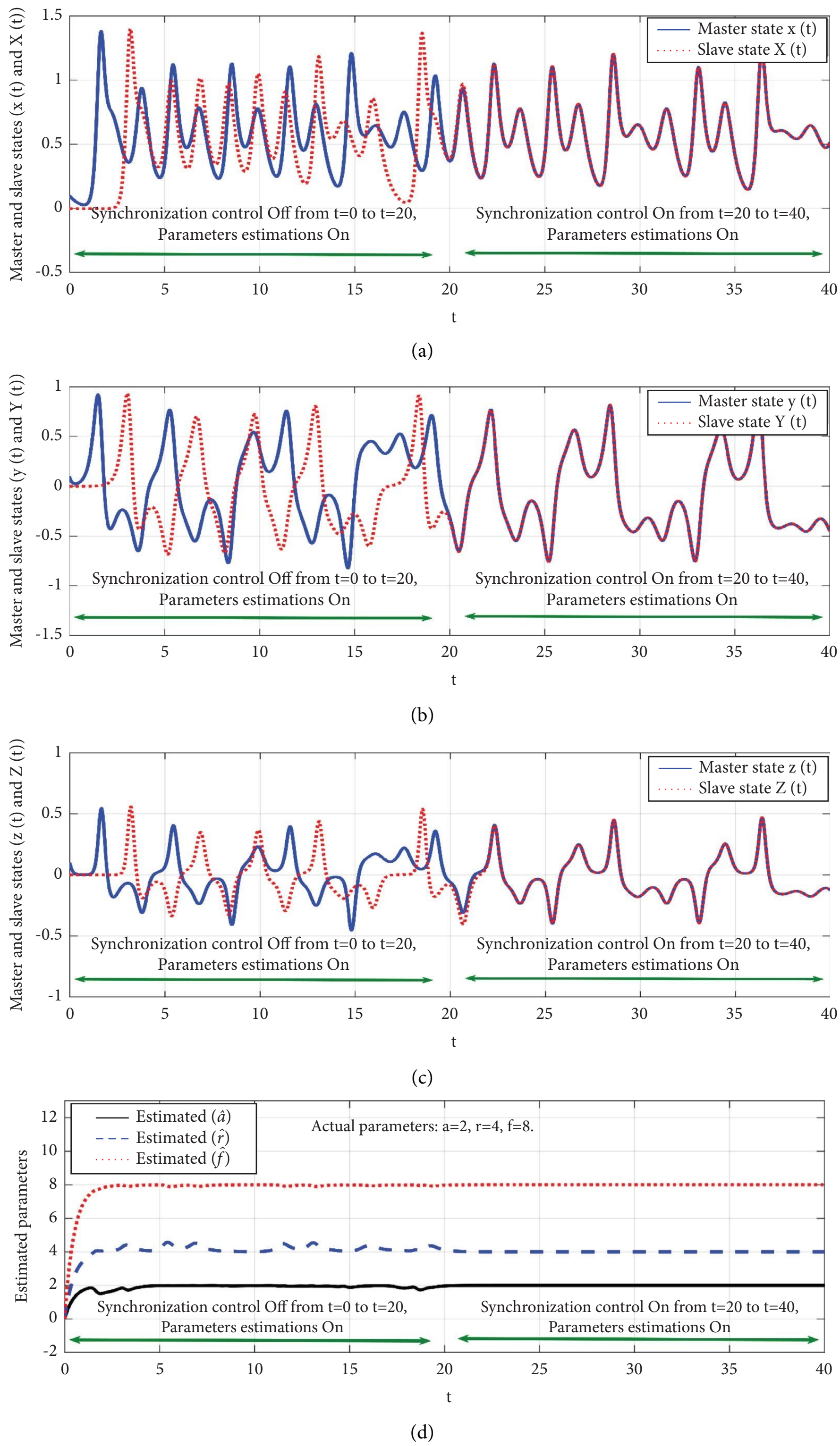

FIGURE 13: The evolution of the chaotic system time response before and after chaos synchronization when the system parameters $a = 2, b = 7, r = 4, g = 11, f = 8, c = 5$, control gains $\alpha_i = \beta_i = 2.0$, $(i = 1, 2, 3)$, and initial conditions $x(0) = y(0) = z(0) = 0.1$, $X(0) = Y(0) = Z(0) = 0.0001, \widehat{a}(0) = \widehat{r}(0) = \widehat{f}(0) = 0.0$. (a–c) the evolution of both the master and slave systems states $x(t), y(t), z(t), X(t), Y(t)$, and $Z(t)$ before chaos synchronization on the interval $0 \le t < 20$ and after chaos synchronization on the interval $20 \le t \le 40$ and (d) the evolution of the system estimated parameters $\widehat{a}, \widehat{r}$, and $\widehat{f}$.

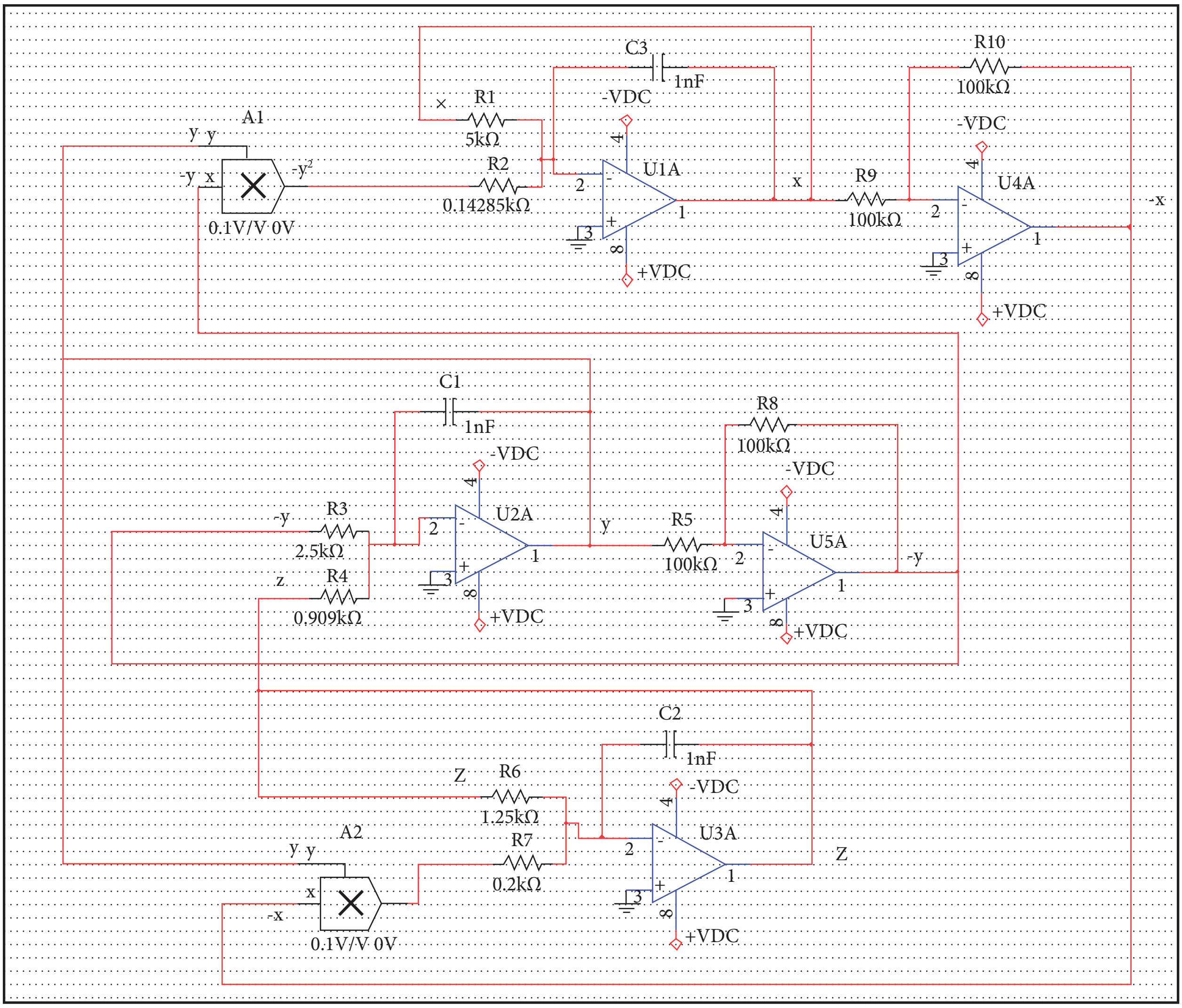

Figure 14: An electronic circuit to simulate the proposed chaotic system given by equation (1) using MultiSim.

$U_1(t) = U_2(t) = U_3(t) = \widehat{a}(t) = \widehat{f}(t) = \widehat{r}(t) = 0)$ on the interval $0 < t < 20$ and after turning on the synchronization controller at $t = 20$ up to $t = 40$. In addition, Figure 12(d) demonstrates the evolution of the estimated parameters $(\widehat{a}(t), \widehat{f}(t)$, and $\widehat{r}(t))$ after turning on the controller at $t = 20$. It is clear from Figures 12(a)–12(c) that the unsynchronized states of the slave system (i.e., $X(t), Y(t)$, and $Z(t)$) on the time interval $0 < t < 20$ have been forced to follow the master system states when the controller is turned on at $t = 20$ (i.e., $X(t) \longrightarrow x(t), Y(t) \longrightarrow y(t)$, and $Z(t) \longrightarrow z(t)$ when $t > 20$). Also, Figure 12(d) demonstrates the exponential convergence of the estimated parameters to the system parameters with time (i.e., $\widehat{a}(t) \longrightarrow a = 2, \widehat{f}(t) \longrightarrow f = 8, \widehat{r}(t) \longrightarrow r = 4$ when $t > 20$).

On the other hand, Figures 13(a)–13(c) show the temporal oscillations of both the master and slave systems before synchronization (i.e., $U_1(t) = U_2(t) = U_3(t) = 0$) on the time interval $0 < t < 20$ and after turning on the synchronization controller at $t = 20$ up to $t = 40$. In addition, Figure 13(d) depicts the evolution of the estimated parameters $(\widehat{a}(t), \widehat{f}(t)$, and $\widehat{r}(t))$ along the time interval $0 < t < 40$. It is clear from Figures 13(a)–13(c) that the unsynchronized states of the slave system (i.e., $X(t), Y(t)$, and $Z(t)$) on the time interval $0 < t < 20$ have been forced to follow the master system states as soon as the controller is turned on at $t = 20$ faster than that in Figures 12(a)–12(c) (i.e., $X(t) \longrightarrow x(t), Y(t) \longrightarrow y(t)$, and $Z(t) \longrightarrow z(t)$ when $t \geq 20$). Moreover, Figure 13(d) demonstrates the abrupt convergence of the estimated parameters to the system parameters when $t \geq 20$ (i.e., $\widehat{a}(t) \longrightarrow a = 2, \widehat{f}(t) \longrightarrow f = 8, \widehat{r}(t) \longrightarrow r = 4$ when ≥ 20).

By comparing Figures 12 and 13, one can notice that in Figure 12, both the control signals and the estimated parameters have been set to zero on the time interval $0 < t < 20$ (i.e., both the adaptive control law and the parameters estimation law have been stopped from $t = 0$ up to $t = 20$), but in Figure 13, the control signals only have been set zero on the time interval $0 < t < 20$ (i.e., the adaptive control law has been stopped from $t = 0$ up to $t = 20$ but the parameters estimation law is activated from $t = 0$ up to $t = 40$). It is clear from Figure 13(d) that the estimated parameters $\widehat{a}(t), \widehat{f}(t)$,

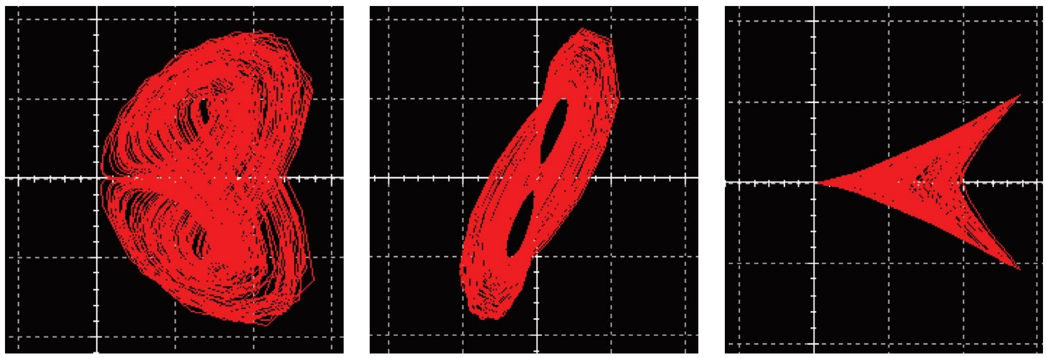

(a) (b) (c)

FIGURE 15: Phase portrait obtained using MultiSim with X: $0.5V$/div, Y: $0.5V$/div, and Z: $0.5V$/div: (a) $x(t)$ versus $z(t)$, (b) $y(t)$ versus $z(t)$, and (c) $x(t)$ versus $z(t)$.

and $\hat{r}(t)$ are very close to the actual system parameters $a = 2, f = 8$, and $r = 4$ on the time interval $0 < t < 20$ even though the adaptive controller has stopped. So, as soon as the controller is turned on at $t = 20$, the correct control signals have been applied to the slave system, which makes it abruptly follows the master system from $t = 20$ up to $t = 40$. Accordingly, to make the slave follows the master system exactly at a short transient time, it is recommended to activate firstly the parameters estimation law before turning on the adaptive control law to avoid the transient time required by the adaptive controller to compute the correct control signals, which was of 4 time steps approximately as shown in Figure 12.

6. Nonlinear Circuit Design

Using MultiSim software (Version 13.0), the proposed chaotic system (1) has been simulated within this section using an electronic circuit consisting of five operational amplifiers (i.e., U1A − U5A) as shown in Figure 14, where three of these amplifiers serve as analog integrators (i.e., U1A − U3A) while the other two are employed as inverting amplifiers (i.e., U4A, U5A). According to this electronic circuit, the straightforward equations of motion that govern the states x, y, and z shown in Figure 14 can be expressed as follows:

$$\begin{aligned}\dot{x} &= \left(-\frac{1}{R_1C_3}\right)x + \left(\frac{R_8}{10R_2R_5C_3}\right)y^2,\\ \dot{y} &= \left(\frac{R_8}{10R_3R_5C_1}\right)y - \left(\frac{1}{R_4C_1}\right)z,\\ \dot{z} &= -\left(\frac{1}{R_6C_2}\right)z + \left(\frac{R_{10}}{10R_7R_9C_2}\right)xy.\end{aligned} \tag{28}$$

Based on equation (28), the circuit components are designed such that $R_1 = 5\text{k}\Omega, R_2 = 0.14285\text{k}\Omega, R_3 = 2.5\text{k}\Omega, R_4 = 0.909\text{k}\Omega, R_5 = 100\text{k}\Omega, R_6 = 1.25\text{k}\Omega, R_7 = 0.2\text{k}\Omega, R_8 = 100\text{k}\Omega, R_9 = 100\text{k}\Omega, R_{10} = 100\text{k}\Omega$, and $c_1 = c_2 = c_3 = 1nF$. Relying on these designed parameters, the circuit output has been visualized using the Multisim oscilloscope as in Figure 15. Figure 15(a) shows the chaotic attractor when the circuit outputs x and y are the input channels to the oscilloscope. In addition, Figure 15(b) shows the phase plane trajectory when the circuit outputs y and z are the input channels to the oscilloscope. Moreover, Figure 15(c) illustrates the phase plane when the circuit outputs x and z are the input channels to the oscilloscope. By comparing Figure 3 with the simulation results in Figure 15, one can notice the typical correspondence between the numerical solutions in Figure 3 and the output of the electronic circuit shown in Figure 15. Accordingly, one can confirm the possible implementation of the introduced chaotic system for different engineering applications such as secure communications, cryptosystems, image processing, and image encryption.

7. Conclusion

A novel three-dimensional autonomous chaotic oscillator having both four linear terms and two quadratic nonlinear terms with six parameters has been studied in this work. The system's dynamics are explored utilizing Lyapunov exponents, bifurcation diagrams, Kaplan–Yorke dimension, time response, and phase plane trajectories. The obtained results demonstrated that the proposed dynamical system may perform periodic, period-n, or chaotic oscillations depending on the designed values of its parameters. In addition, the obtained bifurcation diagrams illustrated that the considered system does not lose its chaotic oscillations for the small fluctuations of one or more of the values of its parameters. Moreover, adaptive control strategies based on Lyapunov's second method of stability have been applied for the purposes of chaos control and chaos synchronization. The numerical simulation proved that the designed adaptive control laws can achieve superior chaos control and master-slave synchronization. Finally, a simple electronic circuit that simulates the system dynamics demonstrated the feasibility of the designed chaotic system for different engineering applications.

Data Availability

The data used to support the findings of this study are included within the article.

Conflicts of Interest

The authors declare that there are no conflicts of interest.

Acknowledgments

The authors would like to thank Taif University, where this work was supported and funded by the Taif University Researchers Supporting Project number TURSP-2020/160, Taif, Saudi Arabia. This work was supported by the Polish National Science Centre, Poland, under the grant OPUS 18 No. 2019/35/B/ST8/00980.

References

[1] Z. Wang, Z. Wei, K. Sun et al., "Chaotic flows with special equilibria," *The European Physical Journal - Special Topics*, vol. 229, no. 6-7, pp. 905–919, 2020.
[2] Z. Wang, Z. Xu, E. Mliki, A. Akgul, V. Pham, and S. Jafari, "A new chaotic attractor around a pre-located ring," *International Journal of Bifurcation and Chaos*, vol. 27, no. 10, Article ID 1750152, 2017.
[3] E. N. Lorenz, "Deterministic nonperiodic flow," *Journal of the Atmospheric Sciences*, vol. 20, no. 2, pp. 130–141, 1963.
[4] O. E. Rössler, "An equation for continuous chaos," *Physics Letters A*, vol. 57, no. 5, pp. 397-398, 1976.
[5] A. Arneodo, P. Coullet, and C. Tresser, "Possible new strange attractors with spiral structure," *Communications in Mathematical Physics*, vol. 79, no. 4, pp. 573–579, 1981.
[6] J. C. Sprott, "Some simple chaotic flows," *Physical Review E - Statistical Physics, Plasmas, Fluids, and Related Interdisciplinary Topics*, vol. 50, no. 2, pp. 647–650, 1994.
[7] G. Chen and T. Ueta, "Yet another chaotic attractor," *International Journal of Bifurcation and Chaos*, vol. 09, no. 7, pp. 1465-1466, 1999.
[8] J. Lü and G. Chen, "A new chaotic attractor coined," *International Journal of Bifurcation and Chaos*, vol. 12, no. 3, pp. 659–661, 2002.
[9] C. Liu, T. Liu, L. Liu, and K. Liu, "A new chaotic attractor," *Chaos, Solitons & Fractals*, vol. 22, no. 5, pp. 1031–1038, 2004.
[10] G. Cai and Z. Tan, "Chaos synchronization of a new chaotic system via nonlinear control," *Journal of Uncertain Systems*, vol. 1, no. 3, pp. 235–240, 2007.
[11] H. K. Chen and C. I. Lee, "Anti-control of chaos in rigid body motion," *Chaos, Solitons & Fractals*, vol. 21, no. 4, pp. 957–965, 2004.
[12] G. Tigan and D. Opris, "Analysis of a 3D chaotic system," *Chaos, Solitons & Fractals*, vol. 36, no. 5, pp. 1315–1319, 2008.
[13] M. S. T. De Freitas, R. L. Viana, and C. Grebogi, "Multistability, basin boundary structure, and chaotic behavior in a suspension bridge model," *Int. J. Bifurcation Chaos*, vol. 14, no. 3, pp. 927–950, 2004.
[14] A. T. Azar and F. E. Serrano, "Robust IMC-PID tuning for cascade control systems with gain and phase margin specifications," *Neural Computing & Applications*, vol. 25, no. 5, pp. 983–995, 2014.
[15] M. F. P. Polo, M. P. Molina, and J. G. Chica, "Chaotic dynamic and control for micro-electro-mechanical systems of massive storage with harmonic base excitation," *Chaos, Solitons & Fractals*, vol. 39, no. 3, pp. 1356–1370, 2009.
[16] F. Alonge, M. Branciforte, and F. Motta, "A novel method of distance measurement based on pulse position modulation and synchronization of chaotic signals using ultrasonic radar systems," *IEEE Transactions on Instrumentation and Measurement*, vol. 58, no. 2, pp. 318–329, 2009.
[17] G. Litak, M. Borowiec, M. I. Friswell, and W. Przystupa, "Chaotic response of a quarter car model forced by a road profile with a stochastic component," *Chaos, Solitons & Fractals*, vol. 39, no. 5, pp. 2448–2456, 2009.
[18] F. Pareschi, G. Setti, and R. Rovatti, "Implementation and testing of highspeed CMOS true random number generators based on chaotic systems," *IEEE Transactions on Circuits and Systems I: Regular Papers*, vol. 57, no. 12, pp. 3124–3137, 2010.
[19] U. Nehmzow and K. Walker, "Quantitative description of robot-environment interaction using chaos theory," *Robotics and Autonomous Systems*, vol. 53, no. 3–4, pp. 177–193, 2005.
[20] C. K. Volos, I. M. Kyprianidis, and I. N. Stouboulos, "Experimental investigation on coverage performance of a chaotic autonomous mobile robot," *Robotics and Autonomous Systems*, vol. 61, no. 12, pp. 1314–1322, 2013.
[21] S. Mondal and C. Mahanta, "Adaptive second order terminal sliding mode controller for robotic manipulators," *Journal of the Franklin Institute*, vol. 351, no. 4, pp. 2356–2377, 2014.
[22] S. Vaidyanathan, A. Sambas, M. Mamat, and W. Mada Sanjaya, "A new three-dimensional chaotic system with a hidden attractor, circuit design and application in wireless mobile robot," *Archives of Control Sciences*, vol. 27, no. 4, pp. 541–554, 2017.
[23] V. T. Pham, C. K. Volos, S. Vaidyanathan, T. P. Le, and V. Y. Vu, "A memristor-based hyperchaotic system with hidden attractors: dynamics, synchronization and circuital emulating," *Journal of Engineering Science and Technology Review*, vol. 8, no. 2, pp. 205–214, 2015.
[24] C. K. Volos, I. M. Kyprianidis, I. N. Stouboulos, E. . Tlelo-Cuautle, and S. Vaidyanathan, "Memristor: a new concept in synchronization of coupled neuromorphic circuits," *Journal of Engineering Science and Technology Review*, vol. 8, no. 2, pp. 157–173, 2015.
[25] C. Li, W. Joo-Chen Thio, H. Ho-Ching Iu, and T. Lu, "A memristive chaotic oscillator with increasing amplitude and frequency," *IEEE Access*, vol. 6, pp. 12945–12950, 2018.
[26] M. Gao, Y. Wang, Y. Wang, and P. Wang, "Experimental investigation of non-linear multi-stable electromagnetic-induction energy harvesting mechanism by magnetic levitation oscillation," *Applied Energy*, vol. 220, pp. 856–875, 2018.
[27] S. M. El-Shourbagy, N. A. Saeed, M. Kamel, K. R. Raslan, M. K. Aboudaif, and J. Awrejcewicz, "Control performance, stability conditions, and bifurcation analysis of the twelve-Pole active magnetic bearings system," *Applied Sciences*, vol. 11, no. 22, Article ID 10839, 2021.
[28] N. A. Saeed, O. M. Omara, M. Sayed, J. Awrejcewicz, and M. S. Mohamed, "Non-linear interactions of jeffcott-rotor system controlled by a radial PD-control algorithm and

eight-Pole magnetic bearings actuator," *Applied Sciences*, vol. 12, no. 13, p. 6688, 2022.
[29] N. A. Saeed, J. Awrejcewicz, A. A. A. Mousa, and M. S. Mohamed, "ALIPPF-controller to stabilize the unstable motion and eliminate the non-linear oscillations of the rotor electro-magnetic suspension system," *Applied Sciences*, vol. 12, no. 8, p. 3902, 2022.
[30] D. Singh, "Ride comfort analysis of passenger body biodynamics in active quarter car model using adaptive neuro-fuzzy inference system based super twisting sliding mode control," *Journal of Vibration and Control*, vol. 25, no. 12, pp. 1866–1882, 2019.
[31] M. Kyriazis, "Applications of chaos theory to the molecular biology of aging," *Experimental Gerontology*, vol. 26, no. 6, pp. 569–572, 1991.
[32] S. Das, D. Goswami, S. Chatterjee, and S. Mukherjee, "Stability and chaos analysis of a novel swarm dynamics with applications to multi-agent systems," *Engineering Applications of Artificial Intelligence*, vol. 30, pp. 189–198, 2014.
[33] S. Vaidyanathan, "3-cells cellular neural network (CNN) attractor and its adaptive biological control," *Int J PharmTech Res*, vol. 8, no. 4, pp. 632–640, 2015.
[34] S. Vaidyanathan, "Adaptive backstepping control of eEnzymes-substrates system with ferroelectric behaviour in brain waves," *Int J PharmTech Res*, vol. 8, no. 2, pp. 256–326, 2015.
[35] I. Suárez, "Mastering chaos in ecology," *Ecological Modelling*, vol. 117, no. 2–3, pp. 305–314, 1999.
[36] W. T. Gibson and W. G. Wilson, "Individual-based chaos: extensions of the discrete logistic model," *Journal of Theoretical Biology*, vol. 339, pp. 84–92, 2013.
[37] C. L. Witte and M. H. Witte, "Chaos and predicting varix hemorrhage," *Medical Hypotheses*, vol. 36, no. 4, pp. 312–317, 1991.
[38] Z. Qu, "Chaos in the genesis and maintenance of cardiac arrhythmias," *Progress in Biophysics and Molecular Biology*, vol. 105, no. 3, pp. 247–257, 2011.
[39] P. Gaspard, "Microscopic chaos and chemical reactions," *Physica A: Statistical Mechanics and Its Applications*, vol. 263, no. 1–4, pp. 315–328, 1999.
[40] V. G., J. M., K. S. Petrov, V. Gáspár, J. Masere, and K. Showalter, "Controlling chaos in the bz," *Nature*, vol. 361, no. 6409, pp. 240–243, 1993.
[41] S. Vaidyanathan, "Adaptive control of a chemical chaotic reactor," *Int J Pharm Tech Res*, vol. 8, no. 3, pp. 377–382, 2015.
[42] S. Vaidyanathan, "Adaptive synchronization of chemical chaotic reactors," *International Journal of ChemTech Research*, vol. 8, no. 2, pp. 612–621, 2015.
[43] N. Li, W. Pan, L. Yan, B. Luo, and X. Zou, "Enhanced chaos synchronization and communication in cascade-coupled semiconductor ring lasers," *Communications in Nonlinear Science and Numerical Simulation*, vol. 19, no. 6, pp. 1874–1883, 2014.
[44] G. Yuan, X. Zhang, and Z. Wang, "Generation and synchronization of feedback-induced chaos in semiconductor ring lasers by injection-locking," *Optik*, vol. 125, no. 8, pp. 1950–1953, 2014.
[45] H. Bi, G. Qi, J. Hu, P. Faradja, and G. Chen, "Hidden and transient chaotic attractors in the attitude system of quadrotor unmanned aerial vehicle," *Chaos, Solitons & Fractals*, vol. 138, Article ID 109815, 2020.
[46] N. A. Saeed, M. S. Mohamed, and S. K. Elagan, "Periodic, quasi-periodic, and chaotic motions to diagnose a crack on a horizontally supported nonlinear rotor system," *Symmetry*, vol. 12, no. 12, p. 2059, 2020.
[47] N. A. Saeed, E. Mahrous, E. Abouel Nasr, and J. Awrejcewicz, "Nonlinear dynamics and motion bifurcations of the rotor active magnetic bearings system with a new control scheme and rub-impact force," *Symmetry*, vol. 13, no. 8, p. 1502, 2021.
[48] N. A. Saeed, M. Ali, H. M. H. Farh, and F. A. Alturki, "Jan awrejcewicz, rub-impact force induces periodic, quasiperiodic, and chaotic motions of a controlled asymmetric rotor system," *Shock and Vibration*, vol. 2021, Article ID 1800022, 27 pages, 2021.
[49] N. A. Saeed, S. I. El-Bendary, M. Sayed, M. S. Mohamed, and S. K. Elagan, "On the oscillatory behaviours and rub-impact forces of a horizontally supported asymmetric rotor system under position-velocity feedback controller," *Latin American Journal of Solids and Structures*, vol. 18, no. 2, p. e349, 2021.
[50] N. A. Saeed, E. M. Awwad, M. A. El-meligy, and E. A. Nasr, "Analysis of the rub-impact forces between a controlled nonlinear rotating shaft system and the electromagnet pole legs," *Applied Mathematical Modelling*, vol. 93, pp. 792–810, 2021.
[51] H. Liang, Z. Wang, Z. Yue, and R. Lu, "Generalized synchronization and control for incommensurate fractional unified chaotic system and applications in secure communication," *Kybernetika*, vol. 48, no. 2, pp. 190–205, 2012.
[52] M. Feki, "An adaptive chaos synchronization scheme applied to secure communication," *Chaos, Solitons & Fractals*, vol. 18, no. 1, pp. 141–148, 2003.
[53] A. A. Zaher and A. Abu-Rezq, "On the design of chaos-based secure communication systems," *Communications in Nonlinear Science and Numerical Simulation*, vol. 16, no. 9, pp. 3721–3737, 2011.
[54] J. Lang, "Color image encryption based on color blend and chaos permutation in the reality-preserving multiple-parameter fractional Fourier transform domain," *Optics Communications*, vol. 338, pp. 181–192, 2015.
[55] X. Zhang, Z. Zhao, and J. Wang, "Chaotic image encryption based on circular substitution box and key stream buffer," *Signal Processing: Image Communication*, vol. 29, no. 8, pp. 902–913, 2014.
[56] A. Sambas, S. Vaidyanathan, E. Tlelo-Cuautle et al., "A 3-D multi-stable system with a peanut-shaped equilibrium curve: circuit design, FPGA realization, and an application to image encryption," *IEEE Access*, vol. 8, pp. 137116–137132, 2020.
[57] R. Rhouma and S. Belghith, "Cryptanalysis of a chaos-based cryptosystem on DSP," *Communications in Nonlinear Science and Numerical Simulation*, vol. 16, no. 2, pp. 876–884, 2011.
[58] M. Usama, M. K. Khan, K. Alghathbar, and C. Lee, "Chaos-based secure satellite imagery cryptosystem," *Computers & Mathematics with Applications*, vol. 60, no. 2, pp. 326–337, 2010.
[59] J. C. Sprott, "Competition with evolution in ecology and finance," *Physics Letters A*, vol. 325, no. 5–6, pp. 329–333, 2004.
[60] D. Guégan, "Chaos in economics and finance," *Annual Reviews in Control*, vol. 33, no. 1, pp. 89–93, 2009.
[61] A. Sambas, S. He, H. Liu, S. Vaidyanathan, Y. Hidayat, and J. Saputra, "Dynamical analysis and adaptive fuzzy control for the fractional-order financial risk chaotic system," *Advances in Differential Equations*, vol. 674, no. 1, pp. 1–12, 2020.

[62] S. Vaidyanathan, A. Sambas, B. Abd-El-Atty et al., "A 5-D multi-stable hyperchaotic two-disk dynamo system with no equilibrium point: circuit design, FPGA realization and applications to TRNGs and image encryption," *IEEE Access*, vol. 9, pp. 81352–81369, 2021.

[63] J. Kengne, J. C. Chedjou, G. Kenne, and K. Kyamakya, "Dynamical properties and chaos synchronization of improved Colpitts oscillators," *Communications in Nonlinear Science and Numerical Simulation*, vol. 17, no. 7, pp. 2914–2923, 2012.

[64] A. Sharma, V. Patidar, G. Purohit, and K. K. Sud, "Effects on the bifurcation and chaos in forced Duffing oscillator due to nonlinear damping," *Communications in Nonlinear Science and Numerical Simulation*, vol. 17, no. 6, pp. 2254–2269, 2012.

[65] A. Sambas, S. Vaidyanathan, T. Bonny et al., "Mathematical model and FPGA realization of a multistable chaotic dynamical system with a closed buttery-like curve of equilibrium points," *Applied Sciences*, vol. 11, no. 2, p. 778, 2021.

[66] A. El-Gohary and I. A. Alwasel, "The chaos and optimal control of cancer model with complete unknown parameters," *Chaos, Solitons & Fractals*, vol. 42, no. 5, pp. 2865–2874, 2009.

[67] S. Effati, J. Saberi-Nadjafi, and H. Saberi Nik, "Optimal and adaptive control for a kind of 3D chaotic and 4D hyperchaotic systems," *Applied Mathematical Modelling*, vol. 38, no. 2, pp. 759–774, 2014.

[68] W. G. Yu, "Stabilization of three-dimensional chaotic systems via single state feedback controller," *Physics Letters A*, vol. 374, no. 13-14, pp. 1488–1492, 2010.

[69] M. Roopaei, B. R. Sahraei, and T. C. Lin, "Adaptive sliding mode control in a novel class of chaotic systems," *Communications in Nonlinear Science and Numerical Simulation*, vol. 15, no. 12, pp. 4158–4170, 2010.

[70] S. Vaidyanathan, "sliding mode control based global chaos control of Liu-Liu-Liu-Su chaotic system," *International Journal of Control Theory and Applications*, vol. 1, no. 2, pp. 15–20, 2012.

[71] S. Mobayen, "Chaos synchronization of uncertain chaotic systems using composite nonlinear feedback based integral sliding mode control," *ISA Transactions*, vol. 77, pp. 100–111, 2018.

[72] J.-B. Wang, C.-X. Liu, Y. Wang, and G. C. Zheng, "Fixed time integral sliding mode controller and its application to the suppression of chaotic oscillation in power system," *Chinese Physics B*, vol. 27, no. 7, Article ID 070503, 2018.

[73] V. Vafaei, H. Kheiri, and A. J. Akbarfam, "Synchronization of fractional order chaotic systems with disturbances via novel fractional-integer integral sliding mode control and application to neuron models," *Mathematical Methods in the Applied Sciences*, vol. 42, no. 8, pp. 2761–2773, 2019.

[74] B. Sarsembayev, K. Suleimenov, B. Mirzagalikova, and T. D. Do, "SDRE-based integral sliding mode control for wind energy conversion systems," *IEEE Access*, vol. 8, pp. 51100–51113, 2020.

[75] S. Vaidyanathan, C. K. Volos, K. Rajagopal, I. M. Kyprianidis, and I. N. Stouboulos, "Adaptive backstepping controller design for the anti-synchronization of identical WINDMI chaotic systems with unknown parameters and its SPICE implementation," *Journal of Engineering Science and Technology Review*, vol. 8, no. 2, pp. 74–82, 2015.

[76] N. Noroozi, M. Roopaei, P. Karimaghaee, and A. A. Safavi, "Simple adaptive variable structure control for unknown chaotic systems," *Communications in Nonlinear Science and Numerical Simulation*, vol. 15, no. 3, pp. 707–727, 2010.

[77] H. Saberi Nik and M. Golchaman, "Chaos control of a bounded 4D chaotic system," *Neural Computing & Applications*, vol. 25, no. 3-4, pp. 683–692, 2014.

[78] S. Vaidyanathan, C. K. Volos, and V. T. Pham, "Analysis, control, synchronization and SPICE implementation of a novel 4-D hyperchaotic Rikitake dynamo System without equilibrium," *Journal of Engineering Science and Technology Review*, vol. 8, no. 2, pp. 232–244, 2015.

[79] G. Chen and X. Dong, *Form Chaos to Order: Perspectives, Methodologies and Applications*, World Scientific, Singapore, 1998.

[80] A. S. Pilovsky, M. G. Rosenblum, and J. Kurths, *Synchronization: A Universal Concepts in Nonlinear Science*, Cambridge University Press, London, UK, 2001.

[81] L. M. Pecora and T. L. Carroll, "Synchronization in chaotic systems," *Physical Review Letters*, vol. 64, no. 8, pp. 821–824, 1990.

[82] T. L. Carroll and L. M. Pecora, "Synchronizing chaotic circuits," *IEEE Transactions on Circuits and Systems*, vol. 38, no. 4, pp. 453–456, 1991.

[83] R. Karthikeyan and V. Sundarapandian, "Hybrid chaos synchronization of four-scroll systems via active control," *Journal of Electrical Engineering*, vol. 65, no. 2, pp. 97–103, 2014.

[84] P. Sarasu and V. Sundarapandian, "Active controller design for the generalized projective synchronization of four-scroll chaotic systems," *International Journal of Systems Signal Control and Engineering Application*, vol. 4, no. 2, pp. 26–33, 2011.

[85] V. Sundarapan and R. Karthikeya, "Hybrid synchronization of hyperchaotic Lorenz and hyperchaotic Chen systems via active control," *Journal of Engineering and Applied Sciences*, vol. 7, no. 3, pp. 254–264, 2012.

[86] S. Vaidyanathan, "Output regulation of the Liu chaotic system," *Applied Mechanics and Materials*, vol. 110–116, pp. 3982–3989, 2012.

[87] S. Vaidyanathan and K. Rajagopal, "Anti-synchronization of Li and T chaotic systems by active nonlinear control," *Commun Comput Inf Sci*, vol. 198, pp. 175–184, 2011.

[88] S. Vaidyanathan, V. T. Pham, and C. K. Volos, "A 5-D hyperchaotic Rikitake dynamo system with hidden attractors," *European Physical Journal: Special Topics*, vol. 224, no. 8, pp. 1575–1592, 2015.

[89] P. Sarasu and V. Sundarapandian, "Adaptive controller design for the generalized projective synchronization of 4-scroll systems," *International Journal of Systems Signal Control and Engineering Application*, vol. 5, no. 2, pp. 21–30, 2012.

[90] V. Sundarapan and R. Karthikeya, "Adaptive anti-synchronization of uncertain Tigan and Li systems," *Journal of Engineering and Applied Sciences*, vol. 7, no. 1, pp. 45–52, 2012.

[91] S. Vaidyanathan, C. Volos, V. T. Pham, and K. Madhavan, "Analysis, adaptive control and synchronization of a novel 4-D hyperchaotic hyperjerk system and its SPICE implementation," *Archives of Control Sciences*, vol. 25, no. 1, pp. 135–158, 2015.

[92] Q. Gan and Y. Liang, "Synchronization of chaotic neural networks with time delay in the leakage term and parametric uncertainties based on sampled-data control," *Journal of the Franklin Institute*, vol. 349, no. 6, pp. 1955–1971, 2012.

[93] X. Xiao, L. Zhou, and Z. Zhang, "Synchronization of chaotic Lur'e systems with quantized sampled-data controller," *Communications in Nonlinear Science and Numerical Simulation*, vol. 19, no. 6, pp. 2039–2047, 2014.

[94] Y. Huang and H. Bao, "Master-slave synchronization of complex-valued delayed chaotic Lur'e systems with sampled-data control," *Applied Mathematics and Computation*, vol. 379, Article ID 125261, 2020.

[95] W. H. Chen, D. Wei, and X. Lu, "Global exponential synchronization of nonlinear time-delay Lur'e systems via delayed impulsive control," *Communications in Nonlinear Science and Numerical Simulation*, vol. 19, no. 9, pp. 3298–3312, 2014.

[96] W. Duan, Y. Li, Y. Sun, J. Chen, and X. Yang, "Enhanced master-slave synchronization criteria for chaotic Lur'e systems based on time-delayed feedback control," *Mathematics and Computers in Simulation*, vol. 177, pp. 276–294, 2020.

[97] S. Rasappan and S. Vaidyanathan, "Global chaos synchronization of WINDMI and Coullet chaotic systems using adaptive backstepping control design," *Kyungpook Mathematical Journal*, vol. 54, no. 2, pp. 293–320, 2014.

[98] S. Vaidyanathan, B. A. Idowu, and A. T. Azar, "Backstepping controller design for the global chaos synchronization of Sprott's jerk systems," *Stud Comput Intell*, vol. 581, pp. 39–58, 2015.

[99] S. Vaidyanathan and A. T. Azar, "Hybrid synchronization of identical chaotic systems using sliding mode control and an application to Vaidhyanathan chaotic systems," *Stud Comput Intell*, vol. 576, pp. 549–569, 2015.

[100] Q. Yao, "Synchronization of second-order chaotic systems with uncertainties and disturbances using fixed-time adaptive sliding mode control," *Chaos, Solitons & Fractals*, vol. 142, Article ID 110372, 2021.

[101] A. Abooee, H. A. Yaghini-Bonabi, and M. R. Jahed-Motlagh, "Analysis and circuitry realization of a novel three dimensional chaotic system," *Communications in Nonlinear Science and Numerical Simulation*, vol. 18, no. 5, pp. 1235–1245, 2013.

[102] K. Deng and S. Yu, "Estimating ultimate bound and finding topological horseshoe for a new chaotic system," *Optik*, vol. 125, no. 20, pp. 6044–6048, 2014.

[103] S. Çiçek, A. Ferikoğlu, and İ. Pehlivan, "A new 3D chaotic system: dynamical analysis, electronic Circuit design, active control synchronization and chaotic masking communication application," *Optik*, vol. 127, no. 8, pp. 4024–4030, 2016.

[104] İ. Pehlivan and Y. Uyaroğlu, "A new 3D chaotic system with golden proportion equilibria: analysis and electronic circuit realization," *Computers & Electrical Engineering*, vol. 38, no. 6, pp. 1777–1784, 2012.

[105] M. Borah, J. P. Singh, and B. K. Roy, P. P. Singh, On the construction of a new chaotic system," *IFAC-PapersOnLine*, vol. 49, no. 1, pp. 522–525, 2016.

[106] F. Yu and C. Wang, "A novel three dimension autonomous chaotic system with a quadratic exponential nonlinear term," *Engineering, Technology & Applied Science Research*, vol. 2, no. 2, pp. 209–215, 2012.

[107] M. Tuna and C. Fidan, "A Study on the importance of chaotic oscillators based on FPGA for true random number generating (TRNG) and chaotic systems," *Journal of the Faculty of Engineering and Architecture of Gazi University*, vol. 33, no. 2, pp. 473–491, 2018.

[108] M. Tuna, M. Alçın, I. Koyuncu, C. Fidan, and I. Pehlivan, "High speed FPGA-based chaotic oscillator design," *Microprocessors and Microsystems*, vol. 66, pp. 72–80, 2019.

[109] M. Tuna, A. Karthikeyan, K. Rajagopal, M. Alcin, and İ. Koyuncu, "Hyperjerk multiscroll oscillators with megastability: analysis, FPGA implementation and a novel ANN-ring-based true random number generator," *AEU - International Journal of Electronics and Communications*, vol. 112, Article ID 152941, 2019.

[110] P. Prakash, K. Rajagopal, I. Koyuncu et al., "A novel simple 4-D hyperchaotic system with a saddle-point index-2 equilibrium point and multistability: design and FPGA-based applications," *Circuits, Systems, and Signal Processing*, vol. 39, no. 9, pp. 4259–4280, 2020.

[111] A. T. Azar and S. Vaidyanathan, "Advances in chaos theory and intelligent control," *Studies in Fuzziness and Soft Computing*, Springer-Verlag, vol. 337, Berlin, Germany, 2016.

[112] H. K. Khalil, *Nonlinear Systems*, Prentice Hall, Hoboken, NJ, USA, 2001.